INTERNATIONAL ATOMIC ENERGY AGENCY
UNITED NATIONS EDUCATIONAL, SCIENTIFIC AND CULTURAL ORGANIZATION
INTERNATIONAL CENTRE FOR THEORETICAL PHYSICS
I.C.T.P, P.O. BOX 586, 34100 TRIESTE, ITALY, CABLE: CENTRATOM TRIESTE

H4-SMR 1012 - 42

AUTUMN COLLEGE ON PLASMA PHYSICS

13 October - 7 November 1997

A Review of Nonlinear Low Frequency Wave Observations in Space Plasmas: On the Development of Plasma Turbulence

B.T. TSURUTANI

Chapter 1

A Review of Nonlinear Low Frequency (LF) Wave Observations in Space Plasmas: On the Development of Plasma Turbulence

Bruce T. TSURUTANI[1], Karl-Heinz GLASSMEIER[2] and
Fritz M. NEUBAUER[3]

[1] *Jet Propulsion Laboratory, California Institute of Technology, 4800 Oak Grove Drive, Pasadena, California 91109 U.S.A.*
[2] *Institut für Geophysik, Technical University of Braunschweig, D-3300 Braunschweig, Germany*
[3] *Universitat zu Köln, Institut für Geophysik und Meteorologie, Köln 41, Germany*

Abstract. As the lead-off presentation for the topic of nonlinear waves and their evolution, we will illustrate some prominent examples of waves in space plasmas. We will describe recent observations detected within planetary foreshocks, near comets and in interplanetary space. It is believed that the nonlinear LF plasma wave features discussed here are part of and may be basic to the development of plasma turbulence. In this sense, this is one area of space plasma physics that is fundamental, with applications to

Because of the large scale sizes of waves in space, multipoint measurements can be made within a single wavelength, as the waves get convected past/propagate past the spacecraft. Of the various wave phenomena in space plasmas, the cometary case is unique because there is a well-define narrow-band "pump" frequency which is essentially at the local ion cyclotron frequency in the instrument (spacecraft) rest frame of reference. At frequencies higher than the "pump", the wave power falls-off with frequency dependences between $f^{-1.9}$ to $f^{-2.1}$, indicative of spectra developing towards, or reaching Kolmogorov or Kraichnan turbulence.

Detailed investigation of waves at higher and lower frequencies than the pump frequency can be used to identify "daughter" and "granddaughter" waves, and thus determine the specific mechanism for the formation of plasma turbulence. Various mechanisms such as wave-wave modulational instabilities, decay instabilities, four-wave processes, wave-particle interactions, dispersion and damping all can affect and be part of this turbulent spectrum (see Chen, 1990). To begin the review, we will first discuss the plasma instabilities that are involved at comets and planetary foreshocks. Because cometary ions initially have almost zero velocity in the spacecraft frame, ion cyclotron waves are detected at the local cyclotron frequency, making this case more tractable (although there is a finite frequency width associated with the resonance, and cyclotron harmonics may also be present, these effects are small in comparison with the broad wave spectrum found at comets). The same basic wave instabilities/modes are observed in planetary foreshocks, regions where back streaming solar wind ion beams can generate LF electromagnetic waves. In this latter case the beam is not necessarily monoenergetic, and therefore the waves are not generated at a single narrow frequency band (the pump is quite broad). Because the spacecraft is not in the same reference frame, there are also strong Doppler shifts which vary with solar wind speed variations. On the other hand, foreshock regions have been crossed hundreds of times by

1.2 Results

The fundamental plasma instability leading to the development of LF plasma waves discussed in this paper is illustrated in Fig. 1, shown for the cometary case. As a comet approaches the sun, heating of the nuclear surface leads to sublimation of its volatile atoms and molecules (~80% H_2O molecules). These particles attain velocities of ~1 km s^{-1} directed radially outward from the nucleus. At 1 AU, the time scale for photoionization and charge exchange (with solar wind protons) to take place is ~10^6 s. Thus, the atoms and molecules typically propagate ~10^6 km before being ionized.

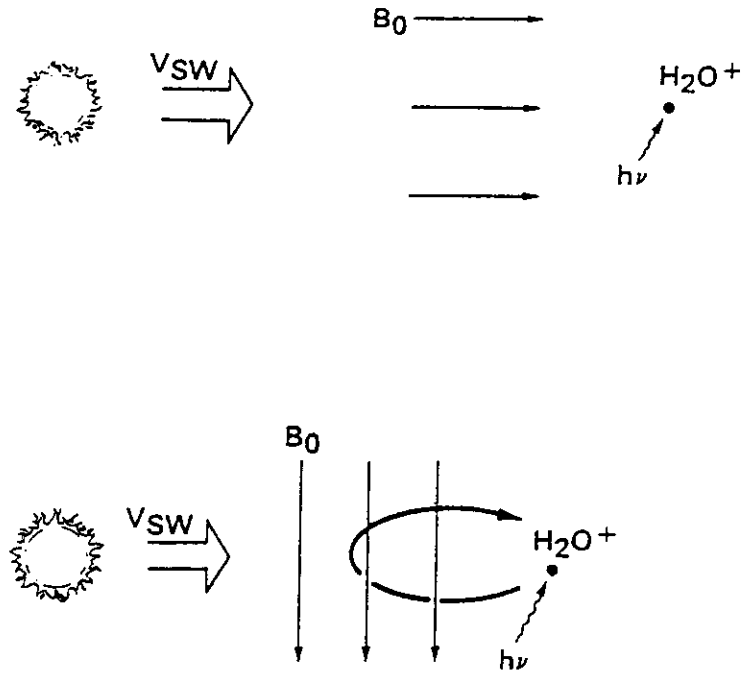

Figure 1: Two extreme cases of cometary ion interaction with the solar wind. In the top

will cause the pickup of the ions, forming a narrow ring with velocity V_{SW} relative to the solar wind, and a convected velocity V_{SW} past the spacecraft. For intermediate field angles, a narrow ring-beam distribution is formed.

All of the above three ion distributions (assuming a sufficiently large beam density) are unstable to resonant wave growth. Discussions of the instabilities can be found in Wu and Davidson (1972), Thorne and Tsurutani (1987), Brinca (1991), Gary (1991) and Roberts and Goldstein (1991). Thorne and Tsurutani (1987) have pictorially illustrated the cyclotron resonance conditions. We have adapted these schematics and present them here in Fig. 2.

The uppermost panel of Fig. 2 represents the case for the upper panel of Fig. 1. In the plasma frame, the ion beam is propagating at a speed V_{SW} towards the sun. The magnetosonic mode phase speed for typical solar wind conditions at 1 AU is $\sim$70 km s^{-1} or $\sim 1/5\ V_{SW}$. Because the left-hand ions are overtaking the right-hand waves, they sense the waves as left-handed. This is called an anomalous Doppler shift. A cyclotron resonance can occur when the resonance condition (top of Fig. 2) is met.

The second panel of Fig. 2 illustrates the ordinary cyclotron resonant interaction. This corresponds closely to the lower panel of Fig. 1. For a predominantly orthogonal pitch angle distribution ($\sim$90°), but with some parallel velocity component, $V_{\|} > V_{ph}$, the ion (parallel to the field) motion causes the wave to Doppler-shift up to the ion cyclotron frequency. Left-hand waves are generated by this instability. The waves propagate in the opposite direction to the particles. This instability is basically the same as the magnetospheric loss cone instability (Kennel and Petschek, 1966). It should be noted, however, that for an exactly 90° pitch angle distribution, the plasma distribution is stable. This is the situation for post-storm magnetospheric ring current particles, where all particles except those at $\sim$90° are strongly pitch angle scattered towards the loss cone.

Energetic electron beams or rings can also generate LF waves, but with the opposite polarization as that for ions. Because the Doppler shift of

$$\omega - \vec{k}\cdot\vec{v} = n\Omega$$

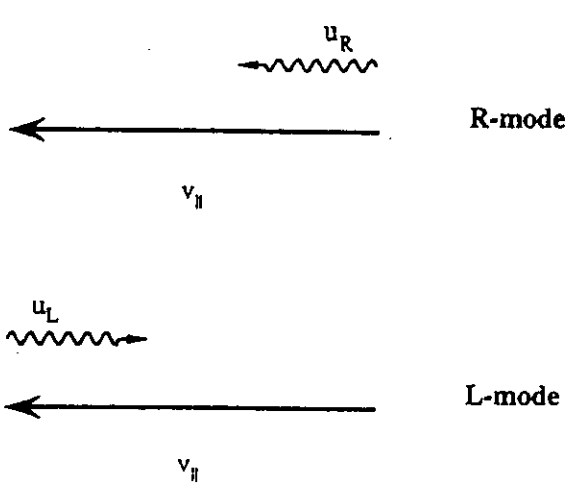

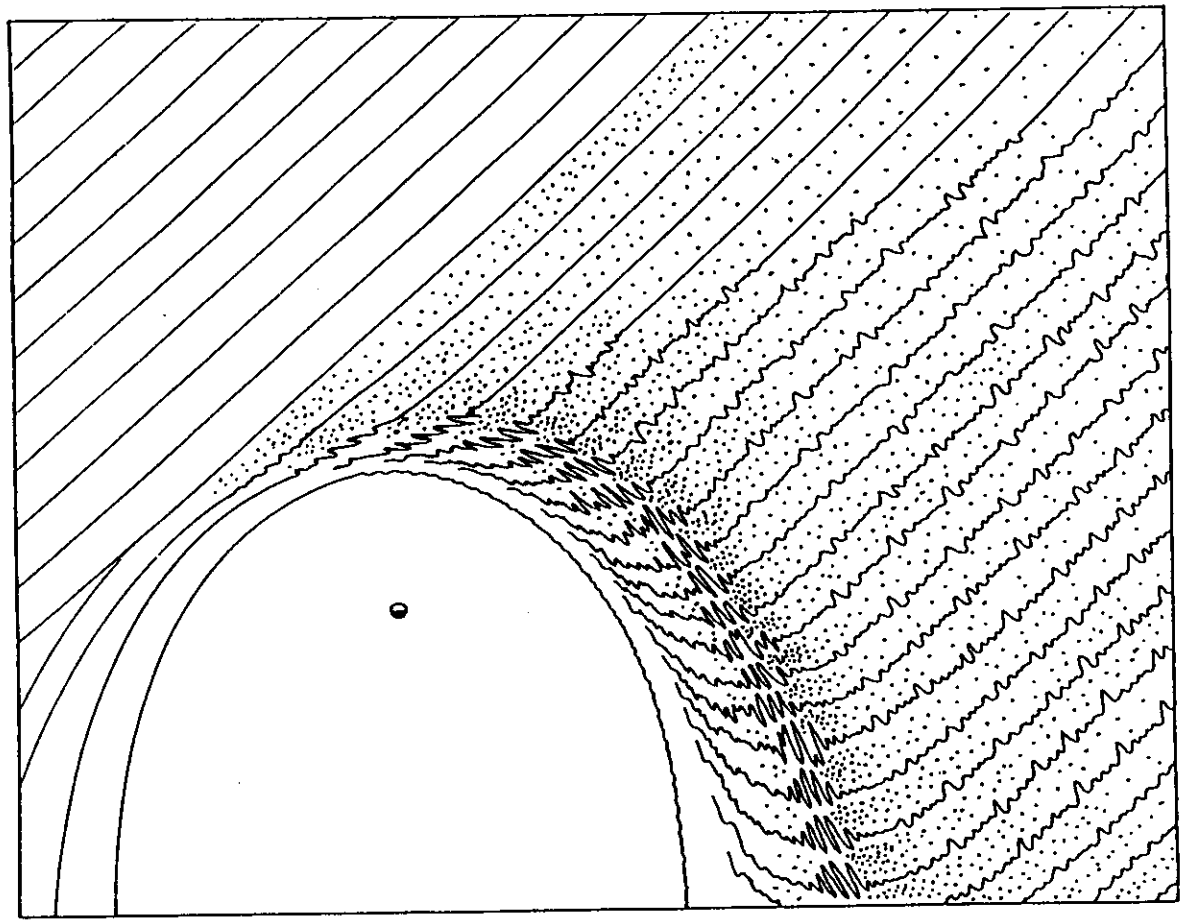

Figure 3: A schematic showing the various waves and particles in a planetary foreshock.

particles, energetic protons coming from the Earth's magnetosphere, and S+, S++ and O+, for Jovian magnetospheric particles). For foreshock cases, there is a spectrum of streaming velocities of the ions, and thus the wave generation is expected to occur at a variety of frequencies. Because the ions and electrons have high velocities relative to the spacecraft frame, there will be strong Doppler shifts and the waves will not be measured at

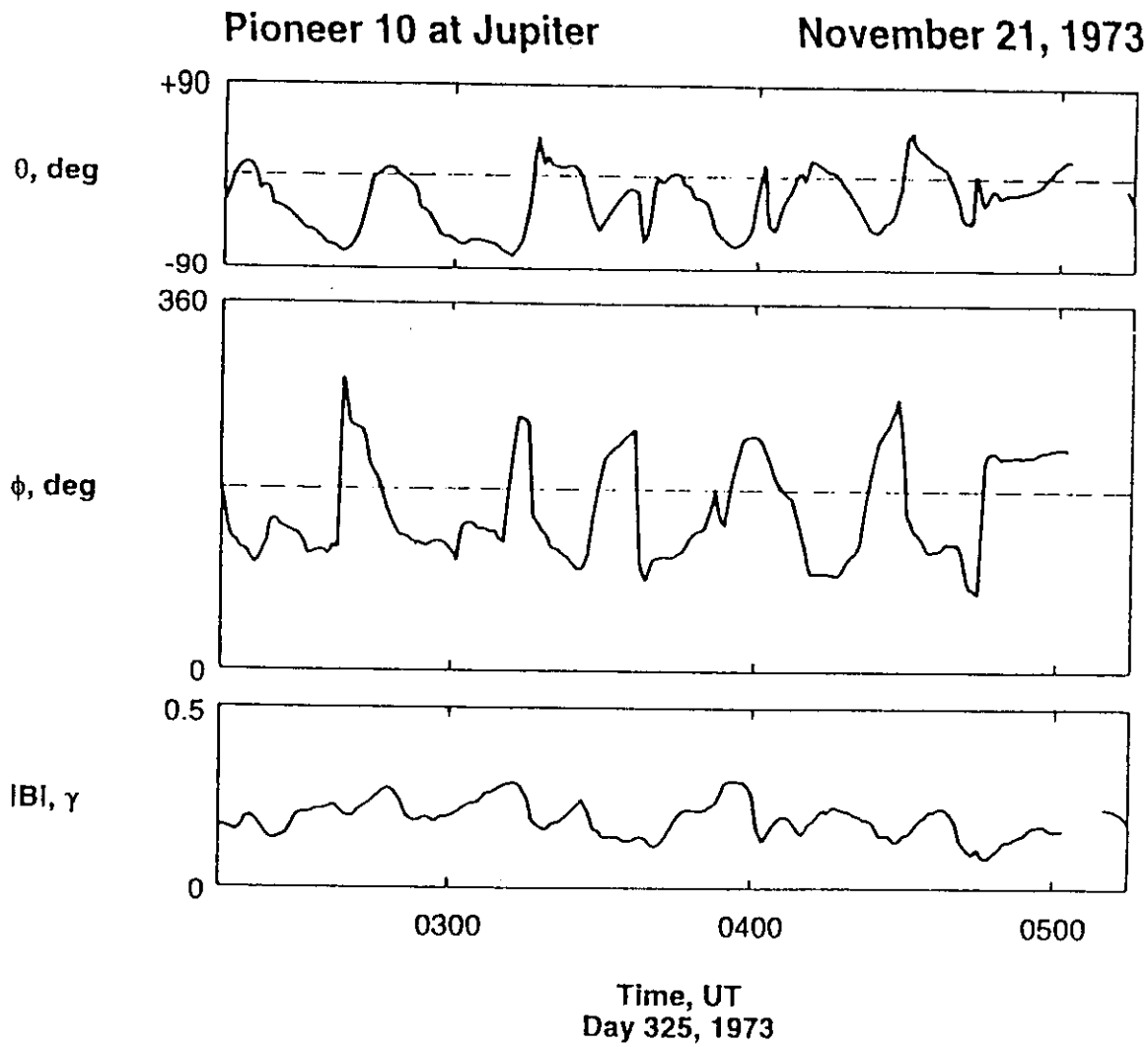

Figure 4: An example of LF waves in the Jovian foreshock during a Pioneer flyby.

Fig. 4), were generated by relativistic $\sim$ MeV electrons. Later, Voyager results (Smith et al., 1983, 1984; Goldstein et al., 1983; 1985; 1986; Smith and

respond to the top panel of the Figure. The right-hand waves would be propagating toward the sun, but because their phase velocities are less than the solar wind speed, they could be anomalously Doppler shifted to appear left-hand polarized in the spacecraft frame. In this case, the right-hand polarized waves would have been generated by an ion beam propagating toward the sun. Conversely, if the waves are detected as right-hand polarized in the spacecraft frame, that would correspond to the third panel of Fig. 4, left-hand polarized waves that are generated by (relativistic) electron beams propagating towards the sun. The second from the top and the bottom panels are not applicable to the foreshock case, because these correspond to large initial particle pitch angles. By definition such particles would have small parallel velocity components, and therefore cannot propagate far into the upstream region.

Some recent results of wave observations in the Jovian foreshock (Tsurutani *et al.*, 1993) are shown in Fig. 5. The Jovian foreshock waves are displayed in the SH coordinate system. In this system, $\hat{x}$ is along the spacecraft-sun line, $\hat{y}$ is in the $\hat{\Omega} \times \hat{x}$ direction, where $\hat{\Omega}$ is the sun's rotation (north) pole, $\hat{z}$ and completes a right-hand system. There are several significant features shown in the Figure. The waves are large amplitude, with the peak-to-peak transverse components as large as $\Delta\vec{B}/|B| \sim 1$ and a compressional component $\Delta|B/|B| \sim 0.5$. Solid horizontal bars in the $|B|$ panel indicate intervals where minimum variance analyses (Sonnerup and Cahill, 1967; Smith and Tsurutani, 1976) have been performed. The angle that $\hat{k}$ subtends relative to $\vec{B}$ is indicated between the third and fourth panels. The labels "L" and "R" correspond to spacecraft frame left-hand and right-hand polarizations, respectively.

The interesting feature of the waves in Fig. 5 is that there is a mix of both (spacecraft frame) right- and left-hand polarizations within the same wave train. The right-hand waves occur when B_x is relatively small, and the left-handed waves when B_x is large. Thus, this is consistent with the right-hand (spacecraft frame) wave cases occurring during intervals when

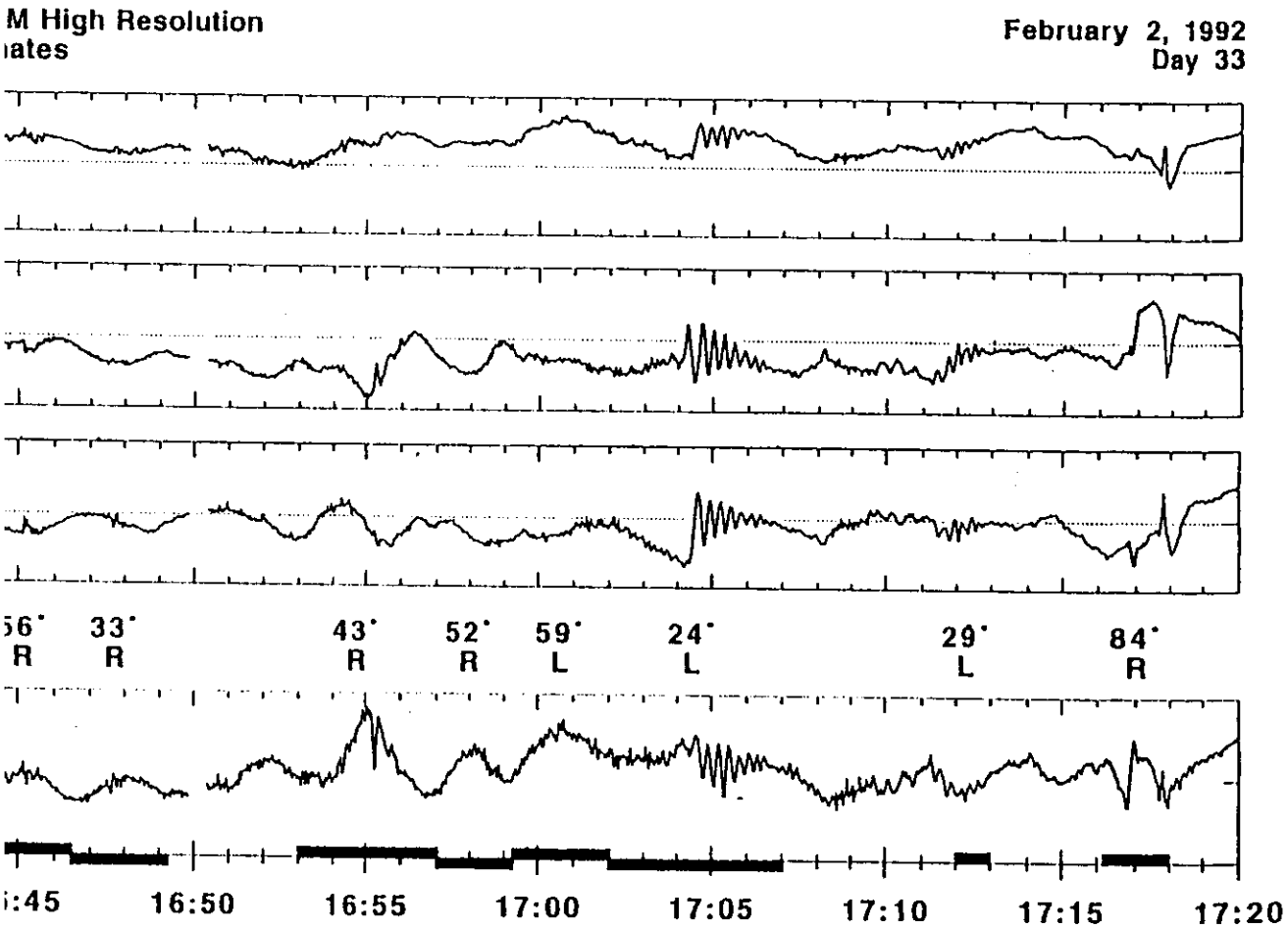

ample of LF waves in the Jovian foreshock during the Ulysses flyby.

ergy. The energies for cyclotron resonance were calculated based on the wave properties and the assumption of generation by a sunward propagating ion beam. It was found that energetic magnetospheric heavy ion beams (S^+, S^{++}, etc.) could not be the source of the waves. The parallel velocity needed for resonance is too low for the particles to propagate into the upstream region. The calculated parallel velocities are lower than the measured solar wind speeds and thus such particles would be convected downstream. Heavy neutral particles (of magnetospheric origin) ionized in the upstream region are a possible source, but the ambient neutral densities would have to be very large to create a beam density that would go unstable. This is because the ionization time scale is very low due to the low solar UV radiation and solar wind ion densities at such large heliospheric distances from the sun (for photoionization and charge exchange processes, respectively). This possibility can thus be eliminated. The last possibility is low energy protons. Substituting numbers into the resonance condition, Tsurutani *et al.* (1993) found that the resonant energy in the spacecraft frame is ~2 keV. This is essentially the energy for reflected solar wind protons. Other intervals of Jovian foreshock data are presently being analyzed to see if all previously reported foreshock waves are consistent with this scenario, or if different ion and/or electron beams must be present during some intervals to be able to explain all of the observations.

The magnetosonic waves plus their attached whistler wave trains have interesting nonlinear features. The whistler packet amplitude decreases with distance upstream of the magnetosonic wave (Fig. 5) [because the wave is propagating towards the sun while being blown back by the solar wind, the "upstream" end of the wave, i.e., the edge along the direction of propagation is detected last in time in the Figure]. Because this amplitude fall-off is linear and not exponential, it is believed that this feature cannot be caused by Landau damping. Dispersion of the whistler mode components of the magnetosonic wave is a more likely possibility. The whistler and the trailing part of the magnetosonic wave are analyzed separately [illegible] minimum variance method. The results are shown in Figs. 6a

has evolved into a wave led by a high frequency whistler packet followed by a nearly linearly polarized structure. The nonlinear "wave" contains both high frequency circular polarization plus low frequency linear polarization as well. We will say more about these features when discussing cometary waves.

Returning to Fig. 5, one other noteworthy feature is the large angles of wave propagation relative to $\vec{B}$. Most cometary intervals analyzed have wave $\vec{k}$ directions at angles greater than 45°. This is even larger than waves in the Earth's foreshock, where typical values are ~10°–15° (Hoppe *et al.* 1981). These large angles have not been explained theoretically. Kojima *et al.* (1989), Kojima (1990) and Karamabadi *et al.* (1994) have been able to produce off-axis wave propagation at small angles (<30°) by assuming a dominance of the ion perpendicular energy (within the distribution function) and also damping of parallel wave modes. However, even larger wave angles, typical of these waves at Jupiter, cannot easily be explained by the above mechanism.

The off-axis propagation feature of magnetosonic waves in foreshocks and at comets is crucial to much of what will be discussed here in this paper. This oblique propagation allows strong wave steepening, nonlinear wave deformation, and as we will see later, the start of possible "turbulent cascades". This is a point that we will return to later.

1.2.2 Comets

An overview of the magnetic field associated with the solar wind interaction with comet Giacobini Zinner is shown in Fig. 7. The coordinate system is GSE where $\hat{x}$ is towards the sun, $\hat{y}$ is in the $\hat{n} \times \hat{x}$ direction where $\hat{n}$ is in the north ecliptic pole direction, and $\hat{z}$ completes the right-hand system. The closest approach to the nucleus occurs at (~1100 UT). The bow wave/shock inbound and outbound crossings occur at ~0930 UT and ~1215 UT and are at a $\sim \pm 10^5$ km distance from the nucleus. The field has been displayed in polar angle coordinates so the "cometary turbulence" is

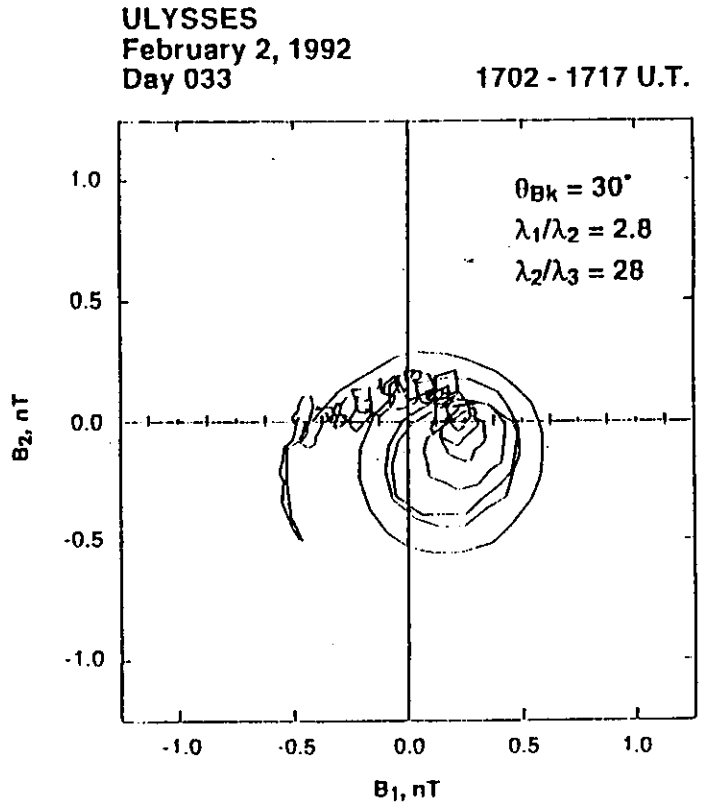
ULYSSES
February 2, 1992
Day 033
1702 - 1717 U.T.
θBk = 30°
λ1/λ2 = 2.8
λ2/λ3 = 28
1.0
0.5
0.0
-0.5
-1.0
B2, nT
-1.0
-0.5
0.0
0.5
1.0
B1, nT

(a)

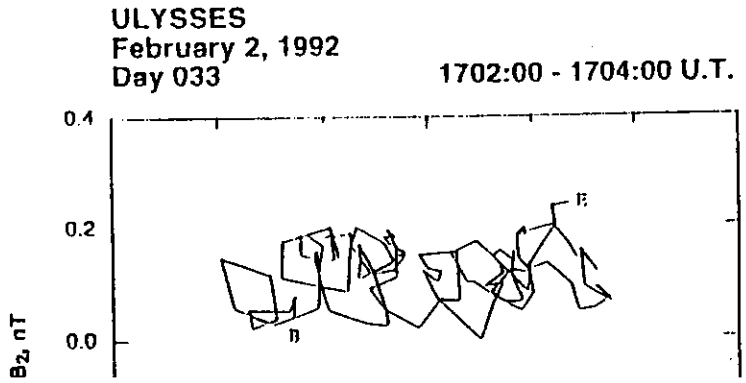
ULYSSES
February 2, 1992
Day 033
1702:00 - 1704:00 U.T.
0.4
0.2
0.0
B2, nT
E
B

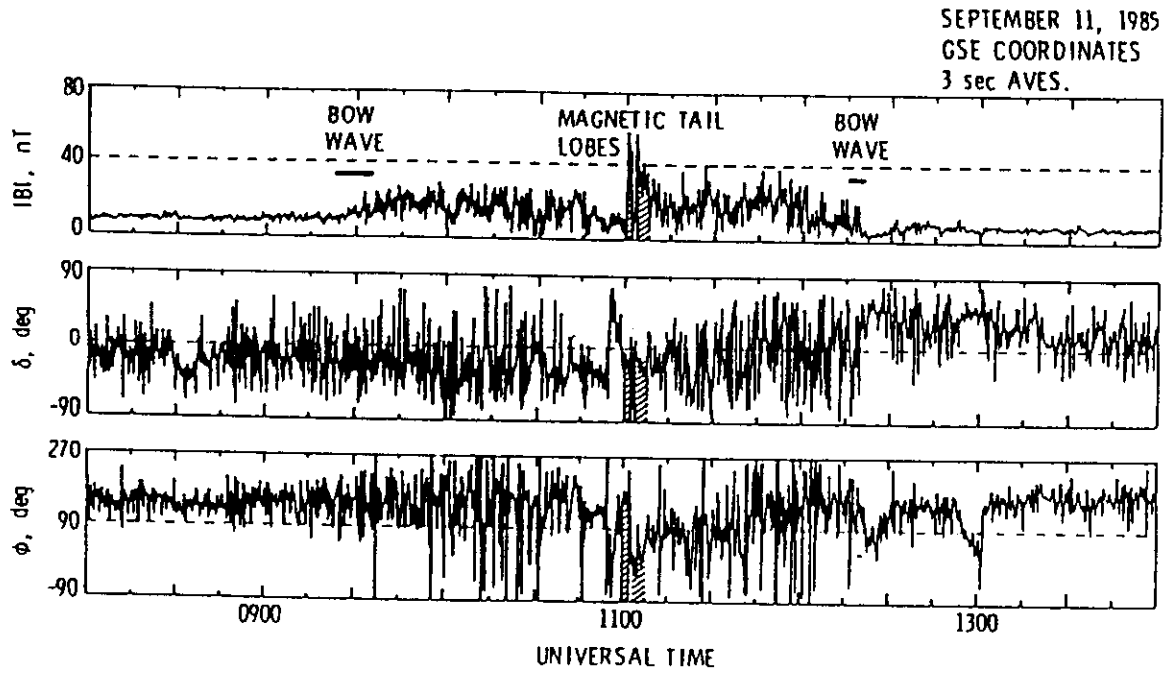

Figure 7: The magnetic field turbulence near comet Giacobini-Zinner.

1993a], Halley [Glassmeier *et al.*, 1989] and Giacobini-Zinner [Tsurutani, 1991]) has been found to be associated with bow shock/wave reflected ions. It is possible that due to the presence of such strong turbulence generated by the pickup ion instabilities, such ions would be rapidly scattered before propagating very far from the shock. Another factor is that cometary bow shocks are quite weak (Smith *et al.*, 1986; Neubauer *et al.*, 1986; 1993b). Due to the solar wind mass loading, the shocks have Mach numbers of only ~2.0 (Schmidt and Wegmann, 1991). Thus, particle reflection from such subcritical shocks would be expected to be quite weak or nonexistent.

The turbulence at comet GZ with measurable wave amplitudes extended to 7×10^5 km (Tsurutani *et al.*, 1987). At Halley, where the bowshock was

imagine a spherical shell of embyronic sinusoidal waves first formed at $\sim 10^6$ km from the nucleus. The idea is these embryonic waves would be sinusoidal and have small amplitudes when first formed. As the waves sunward of the comet get convected by the solar wind towards the nucleus, the continuous formation of cometary ions sunward of the comet gives additional free energy for continual amplitude growth. Thus the amplitudes will increase into the nonlinear range where phase-steepening (Cohen and Kulsrud, 1974; Tsurutani *et al.*, 1987) will occur. This is illustrated in the next-to-bottom sketch. As the waves get driven harder or evolve further, they form whistler packets, shown in the third from the bottom panel. The mechanism for this packet generation will be discussed later. Finaly, very close to the bow shock, as the train of magnetosonic waves plus whistler packets expand further, they will run into their neighbor waves. At this point in time, some very interesting physical processes may occur. Wave-wave interactions such as the modulational or decay instabilities could lead to the creation of daughter or granddaughter waves, forming a fully turbulent plasma. However, we will show later that the waves around comet GZ and GS occupied too small of a spatial region to develop into a fully turbulent state (they quickly get convected into the downstream region). On the other hand, the comet Halley turbulence region was far larger (due to a much higher comet neutral gas production rate), and the measured Halley turbulence does not have well defined wave structures such as those at GS or GZ (Glassmeier *et al.*, 1989). We are presently examining Halley to determine if such second or third generation waves are present or not.

The power spectra of the transverse magnetic field components of three comets are shown in Fig. 9. The wave interval for each comet was selected just upstream of its bow shock/wave, so that the development of "turbulence" could be compared for similar scales. The power spectra of the two transverse components were averaged. From the Figure, first note that the power spectra at each comet is strongly peaked at $\sim 10^{-2}$ Hz, the water group ion cyclotron frequency. This is the "pump" wave for the cascade system. At frequencies higher than the pump, the power spectral fall-off

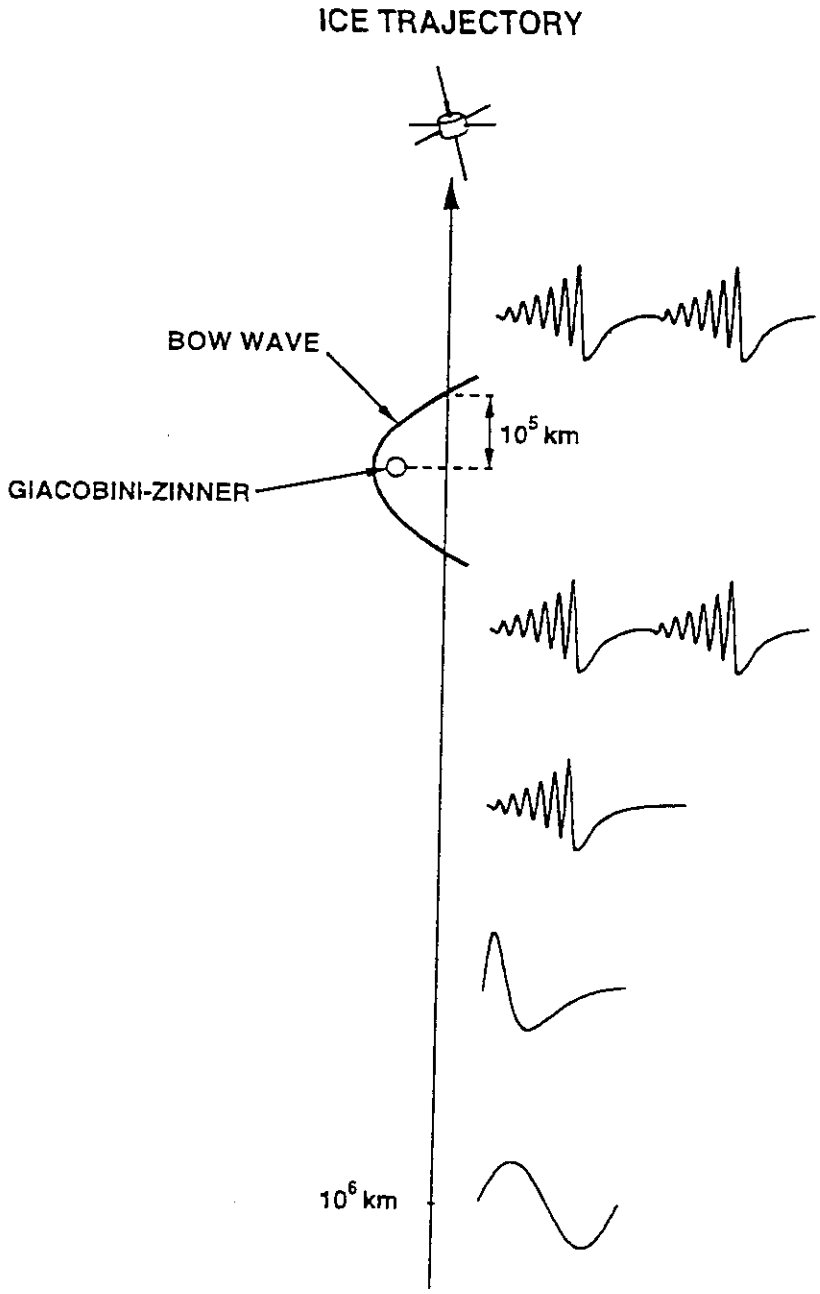
ICE TRAJECTORY
BOW WAVE
10^5 km
GIACOBINI-ZINNER
10^6 km

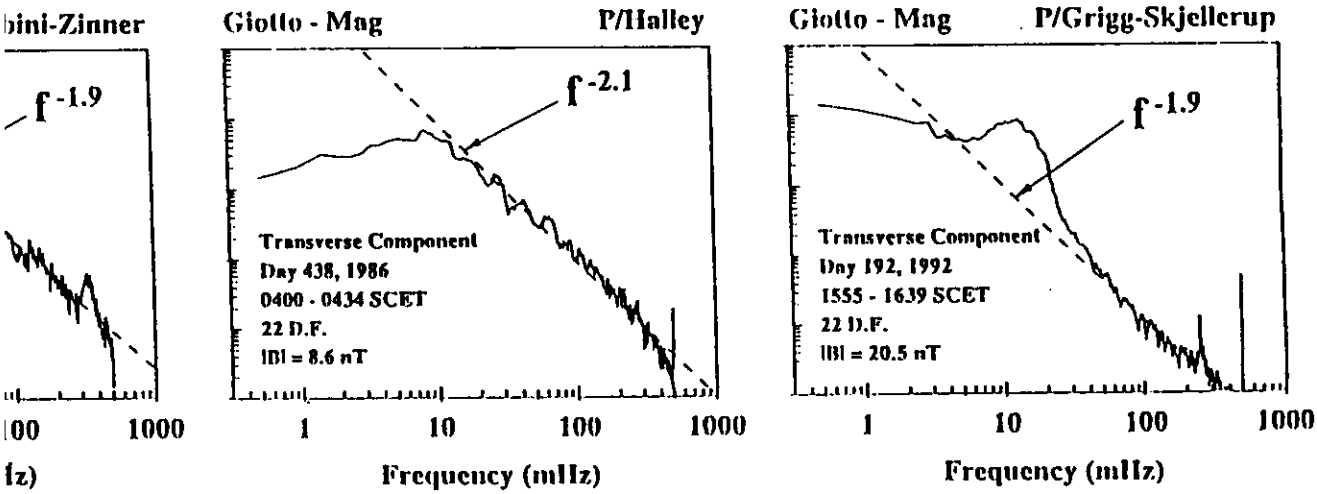

b) c)

power spectra of the transverse components of the magnetic fields for
ni-Zinner, Halley and Grigg-Skjellerup.

this time, the correct picture is not clear. Embryonic sinusoidal waves were not found at comet Halley as well.

The polarizations of the two wave "breakings" are shown in minimum variance coordinates in Figs. 11 and 12. The leading portions correspond to planar waves with circular polarization. In both cases, the wave is left-hand polarized in the spacecraft frame, consistent with a right-hand wave that has been anomalously Doppler shifted to left-hand polarization by the solar wind convective flow. The waves are propagating at substantial angles relative to the ambient field, 29° and 40°, respectively.

As waves develop further, we have the situation shown in Figs. 13 and 14. This example takes place at a distance of $\sim 2.5 \times 10^5$ km from the nucleus. This wave corresponds closely to the next to bottom schematic of Fig. 8. In Fig. 13, the trailing part of the magnetosonic wave (from 718:20 to 719:09, or from the beginning of the interval to point 1), is linearly polarized. This is indicated by the lack of phase rotation from points B to 1 in Fig. 14, and is due to a purely compressive component of B_3 (and $|B|$) [see Fig. 13]. Note that this polarization is not the typical transverse linear

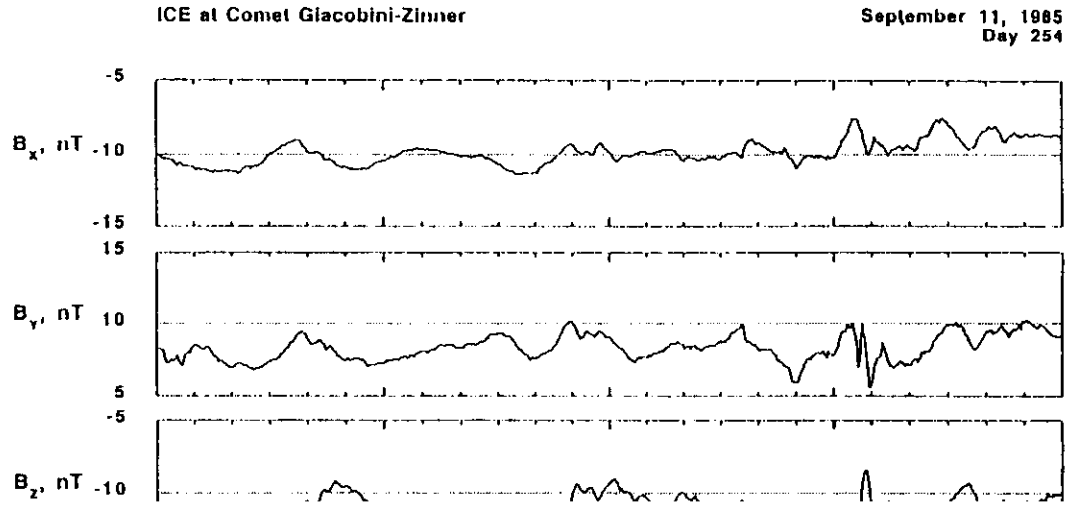

polarization that one ordinarily encounters. In this case, the polarization is due to a purely compressive component (wave-particle interaction will not result in pitch angle scattering, but particle mirroring).

Almost all of the 360° phase rotation of the wave occurs at the leading edge, between points 1 and 4 in the two Figures. In fact, there is ~270° of phase rotation from point 2 to 3, within 2 to 3s of the 100s wave. In terms of wave power, such as the power spectra shown in Fig. 9, this represents some of the high frequency power in the "cascade" part of the spectrum. The wave is planar and left-hand circularly polarized in the spacecraft frame.

Figure 15, is a example of a wave at 1.6×10^5 km from the nucleus of GZ. The wave not only has developed into a nonlinear wave with a strong ($\Delta|B|/|B| \sim 1.0$) compressive factor (from 6.5 nT to almost 13.0 nT), and a region of sharp phase rotation (~ points 1–4), but some small amplitude upstream whistlers are present as well.

Even closer to the comet nucleus, we find a fully developed train of

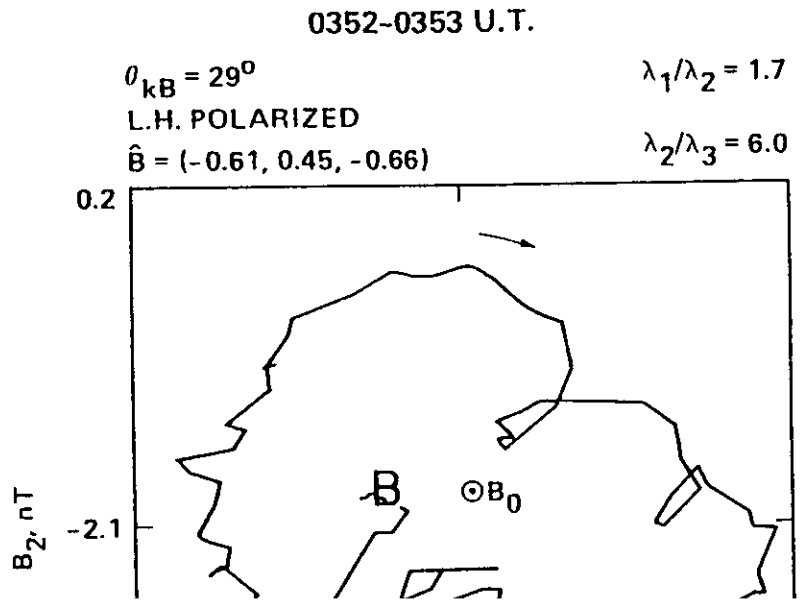

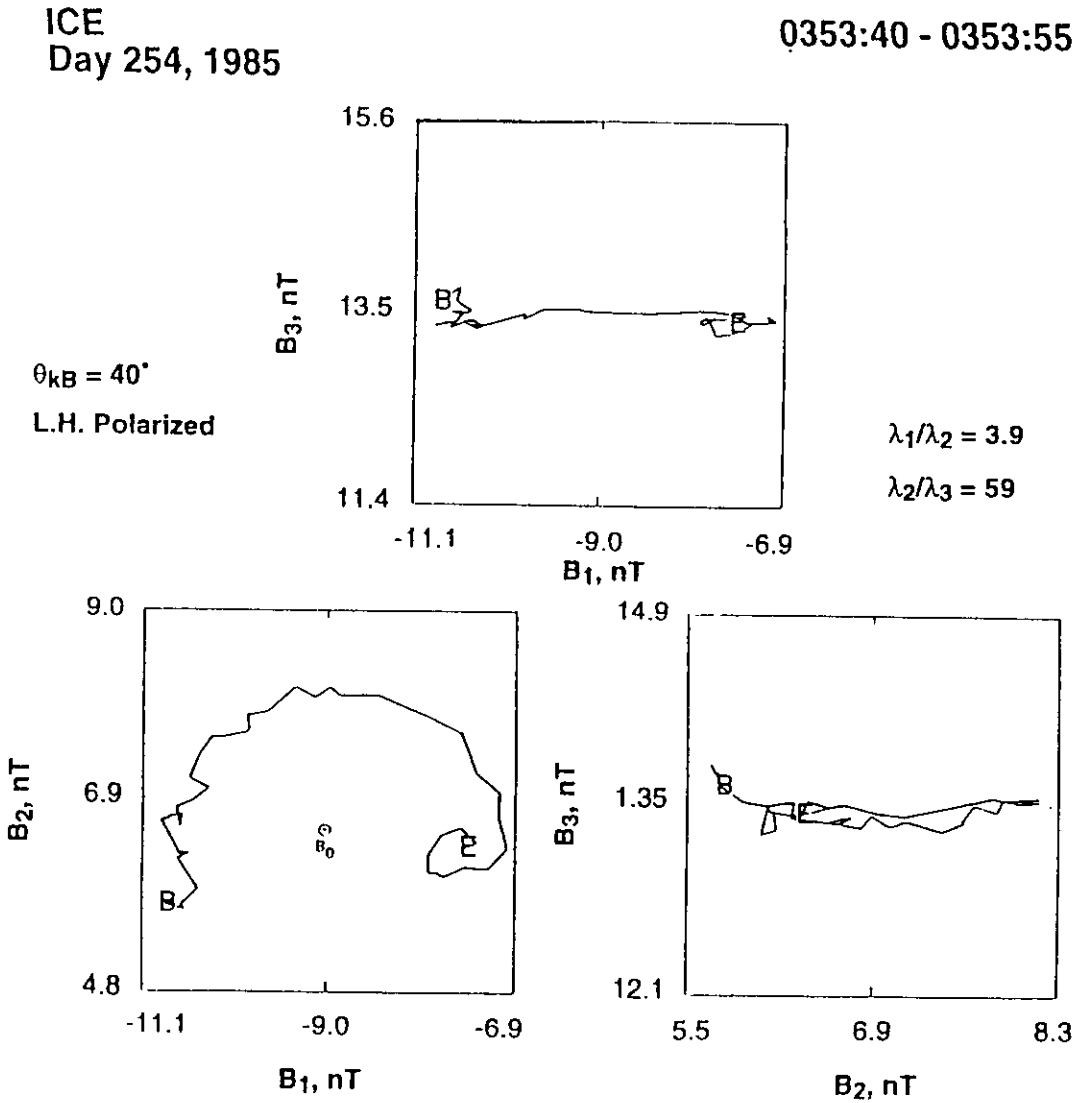

Figure 12: Same as for Fig. 11.

nonlinear waves plus their whistler packet precursors. This is shown in

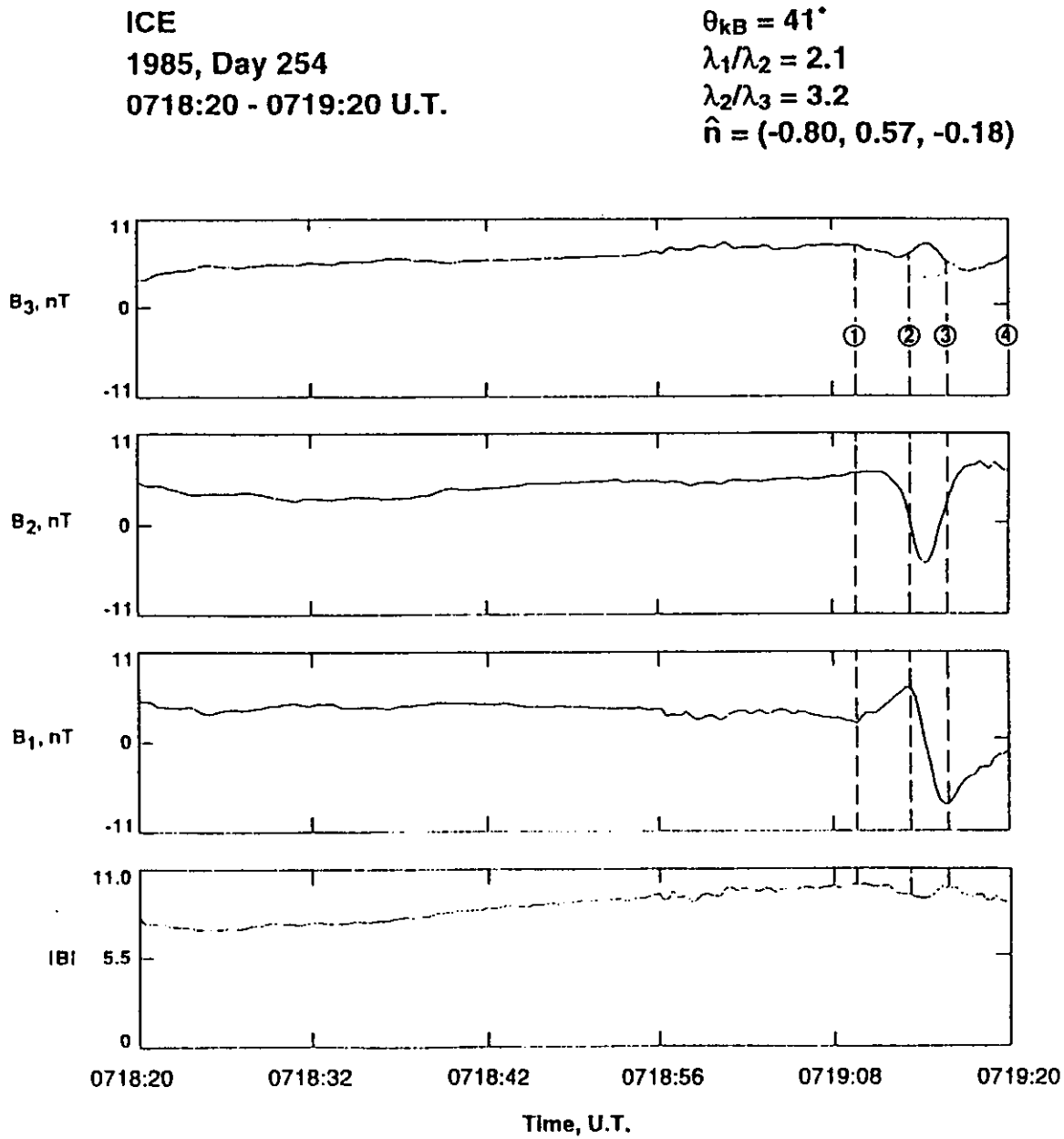
ICE
1985, Day 254
0718:20 - 0719:20 U.T.
θkB = 41°
λ1/λ2 = 2.1
λ2/λ3 = 3.2
n̂ = (-0.80, 0.57, -0.18)
B3, nT
B2, nT
B1, nT
IBI
11
0
-11
11.0
5.5
0
①
②
③
④
0718:20
0718:32
0718:42
0718:56
0719:08
0719:20
Time, U.T.

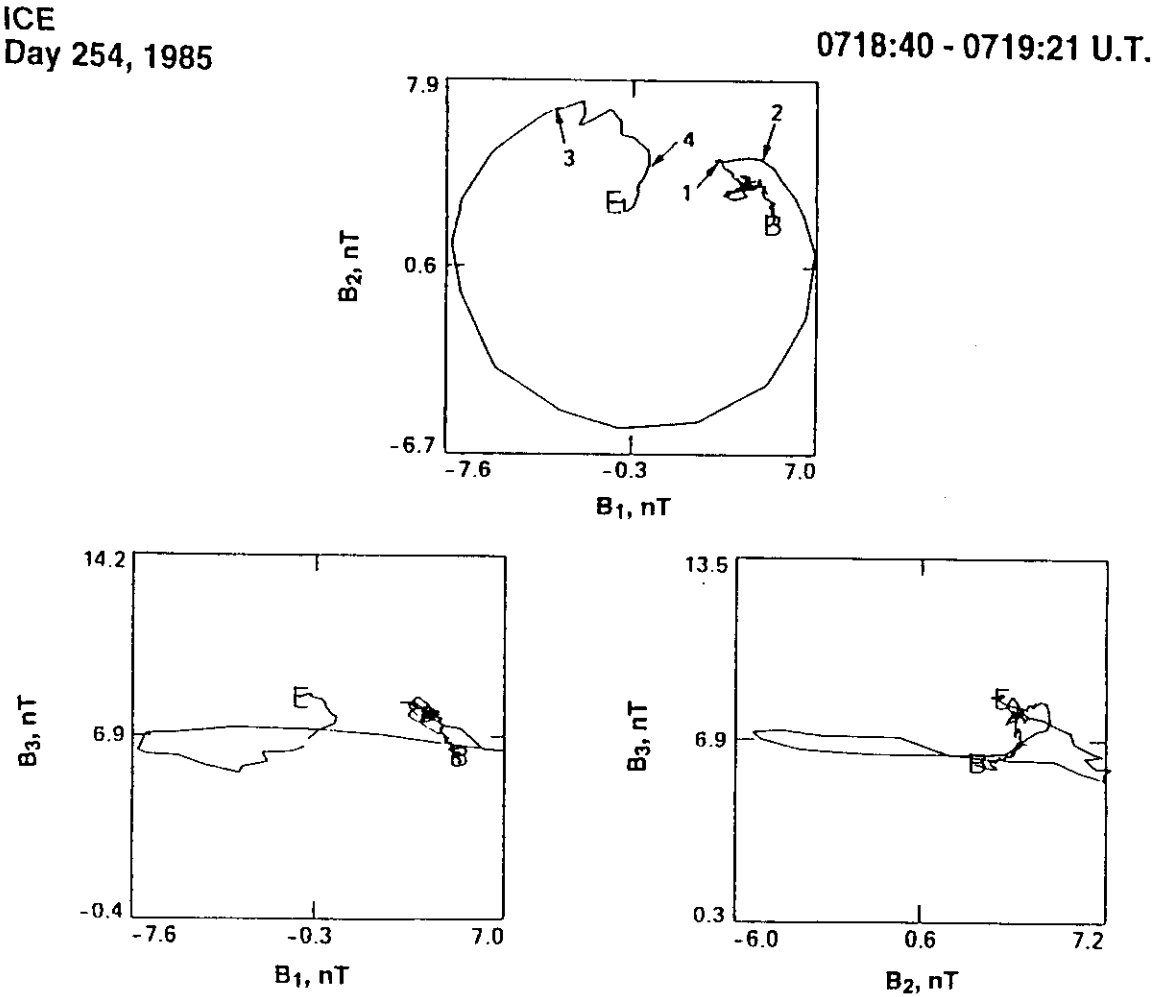

Figure 14: The hodogram for the wave event in Fig. 13. Most (~270°) of the phase rotation occurs at the leading edge of the wave.

ment of magnetosonic waves. This example was taken at a distance of $\sim 1.6 \times 10^5$ km from the nucleus. At 0827 UT there is a decrease in $|B|$

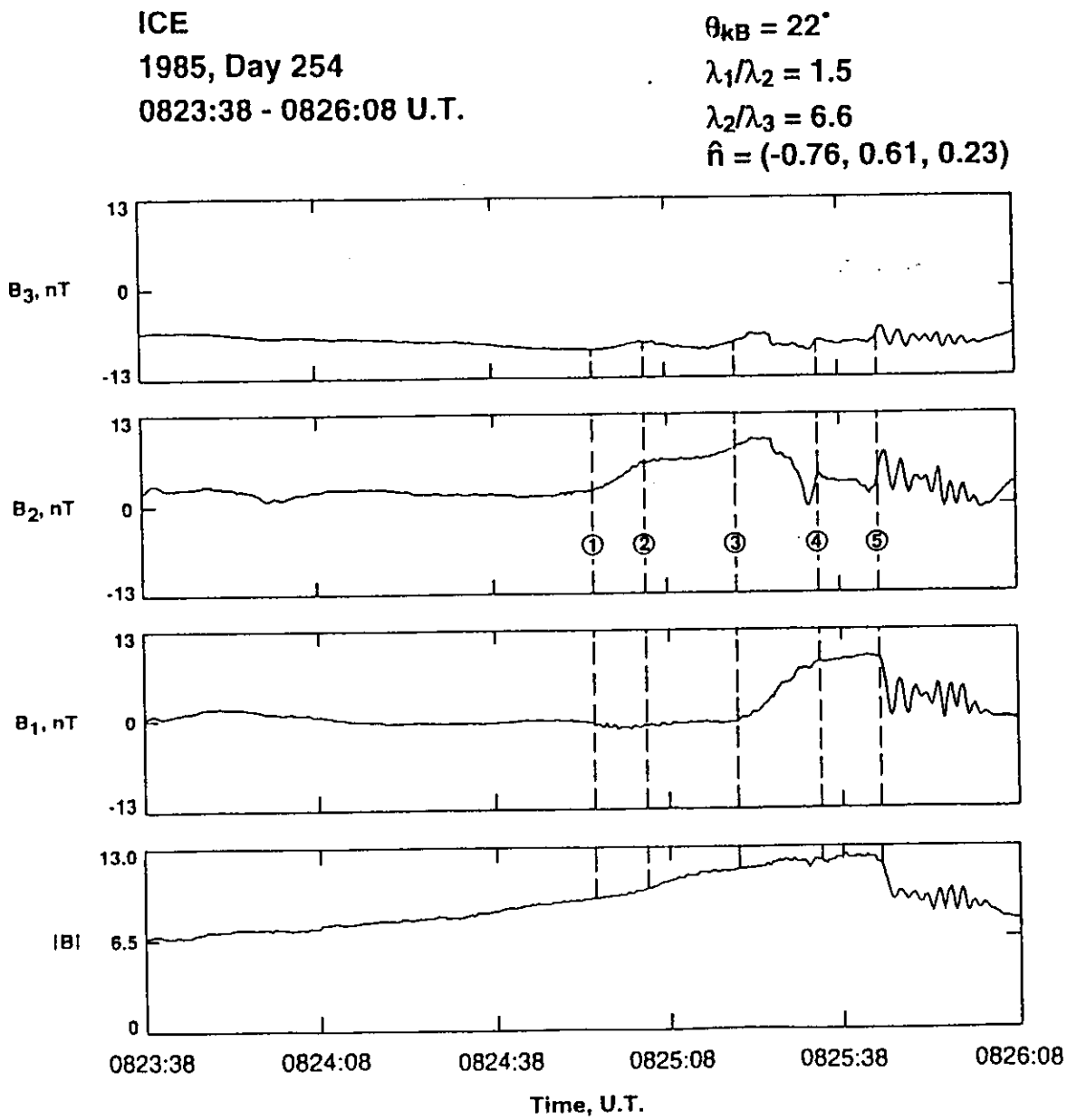

Figure 15: Further development of G-Z nonlinear waves as ICE approaches the comet

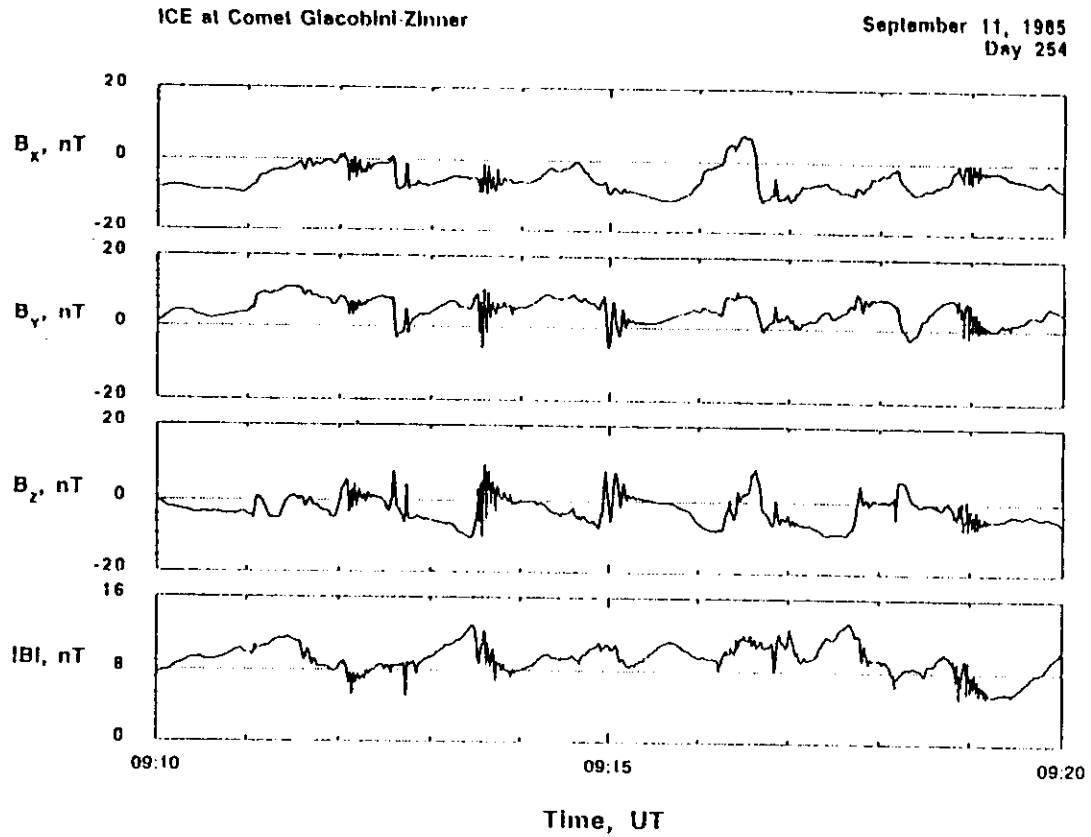

Figure 16: A fully developed train of nonlinear waves detected at a distance $\sim 10^5$ km from the comet nucleus. Whistler precursors are a common feature at this distance.

being anomalously Doppler-shifted by the solar wind convection flow. We cannot tell which of the two possibilities is the correct one. However if the former one is correct, this wave may be a daughter wave from a decay instability (Tsurutani *et al.*, 1990). The wave has an ~8s period.

From point 3 to the end of the interval, 0827:20 UT, there is a sharp wave phase rotation. It is left-hand circularly polarized in the spacecraft

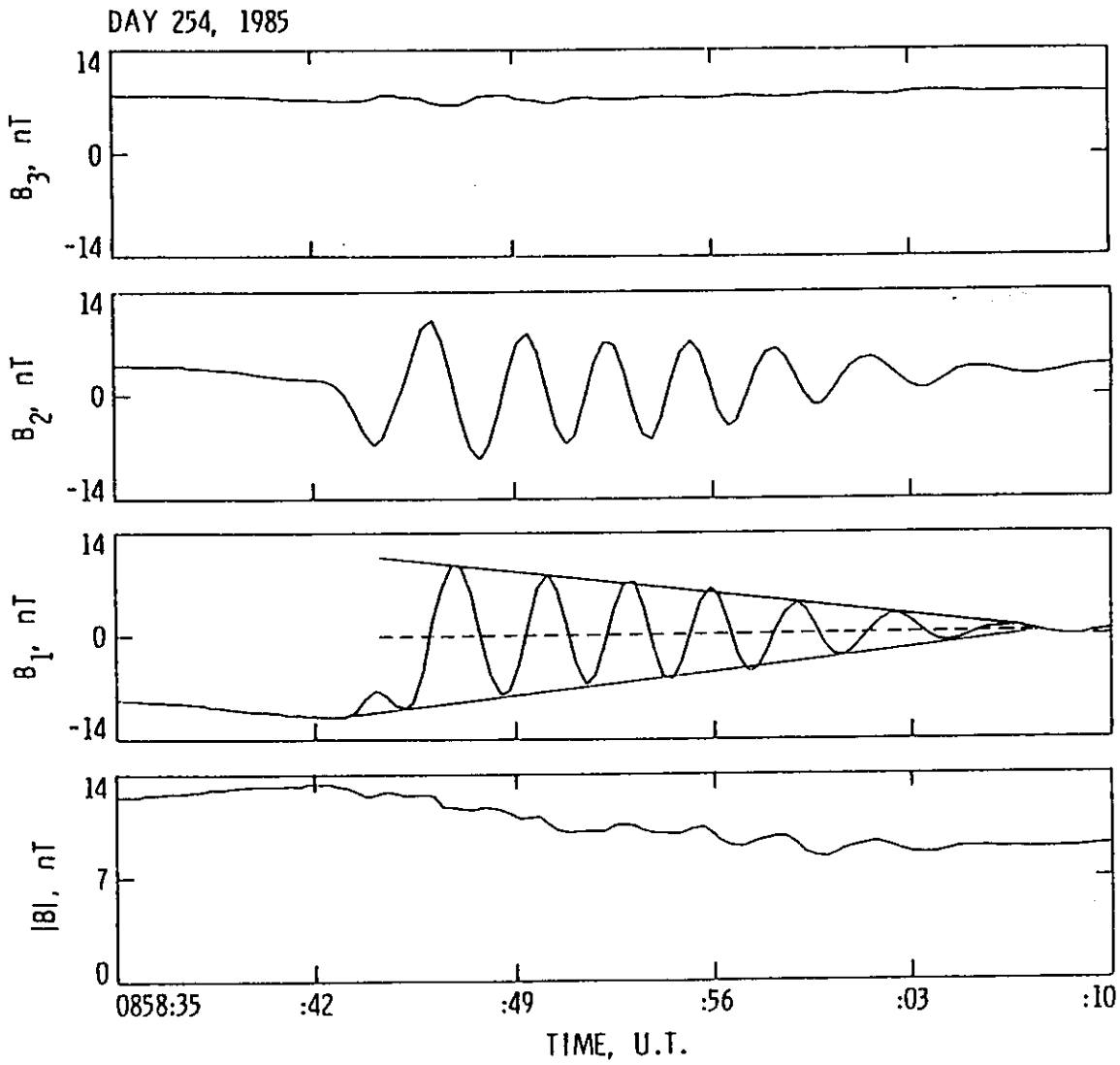

Figure 17: An example of a whistler precursor.

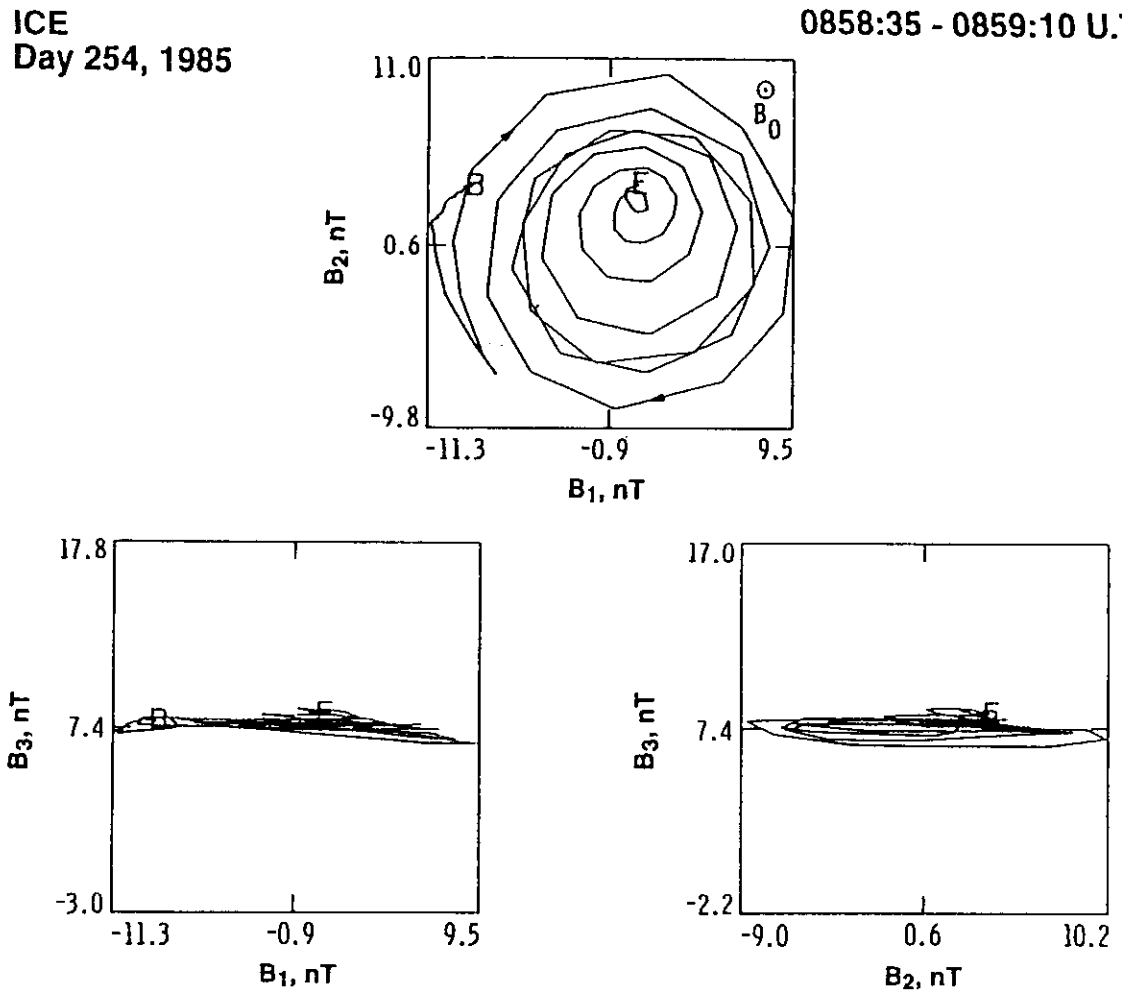

Figure 18: The hodograms for the Fig. 17 event. The whistler packet is plane-polarized and its amplitude decreases linearly with increasing upstream distance from the magnetosonic wave.

are of prime interest to us here.

One example of turbulence-like magnetic field structure is given in

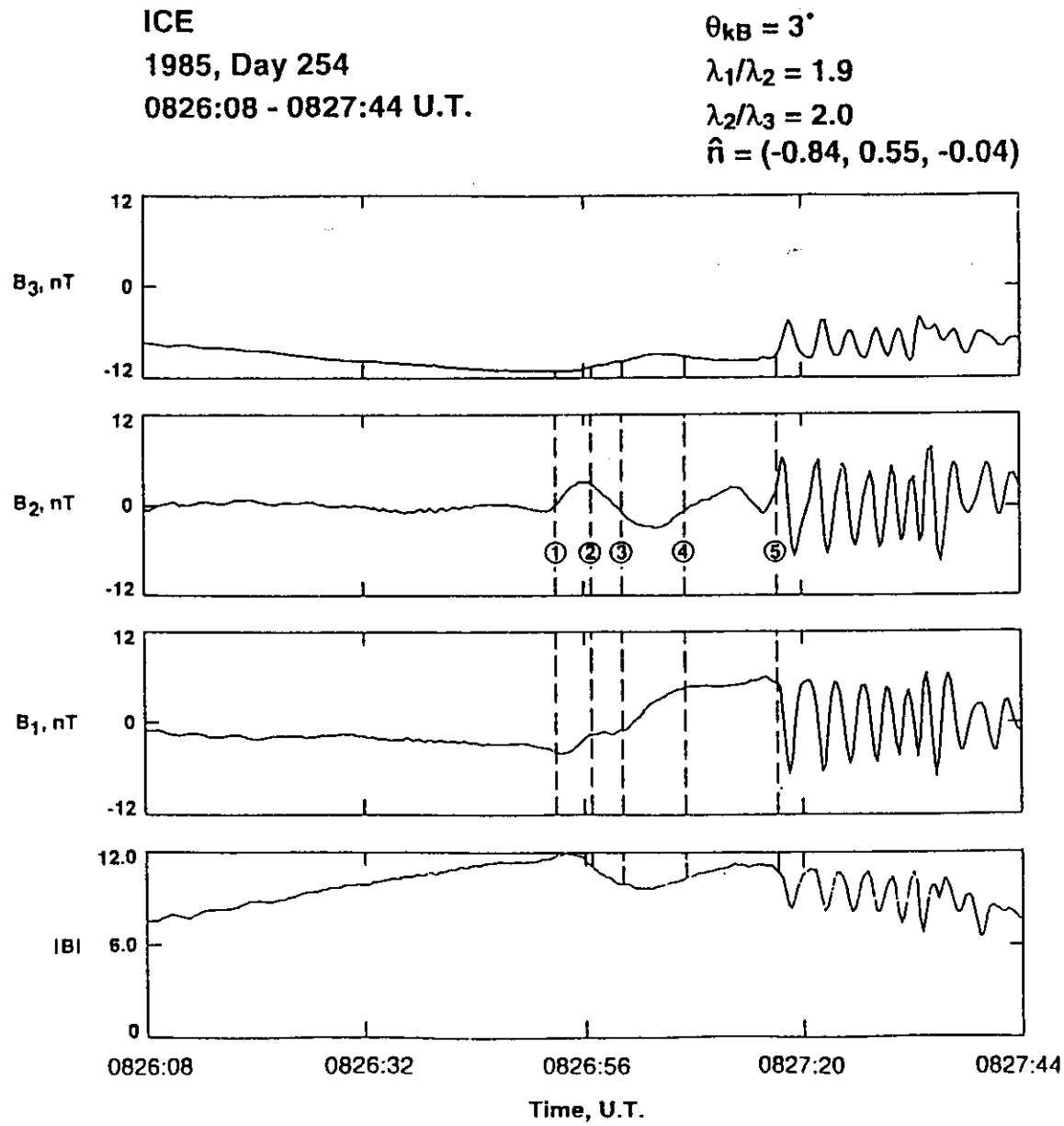

Figure 19: A more complex magnetosonic wave that has appearances of splitting in half.

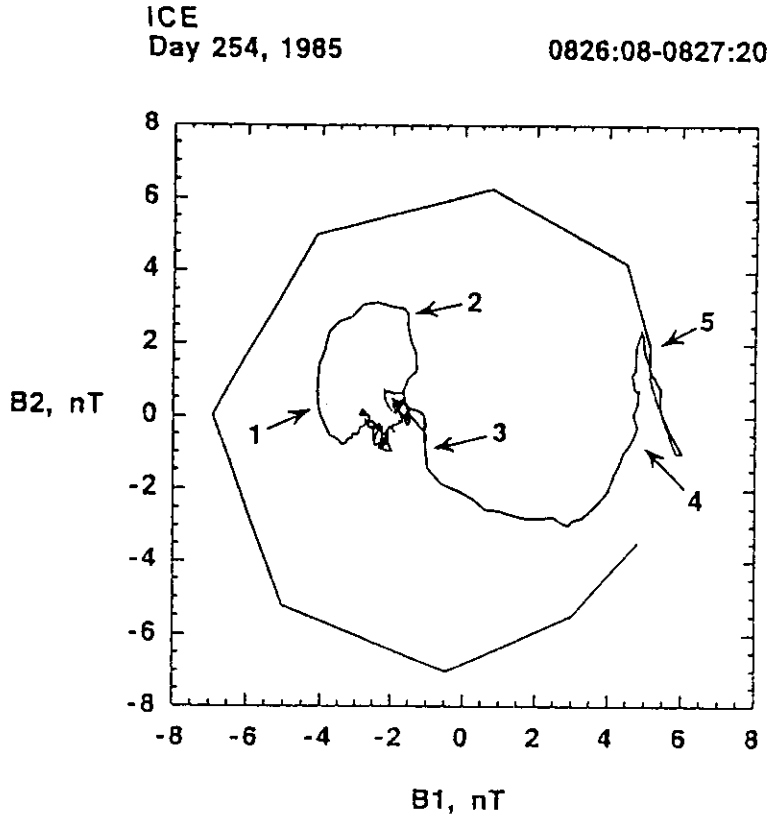

Figure 20: A $B_1 - B_2$ hodogram of the center portion of the interval of Fig. 19. A wave with the opposite polarity, right-hand circularly polarized in the spacecraft frame, is present. This may be the product of a decay instability.

vice versa) to V_{SW}. On the other hand, one cannot rule out the possibility that the two waves have the same plasma frame polarity, one propagating towards the sun and the other away. Further research is needed to resolve this problem.

From the time intervals given in Fig. 25, the wave periods are ~10s and ~7s respectively. Thus, the wave power would fall into the second

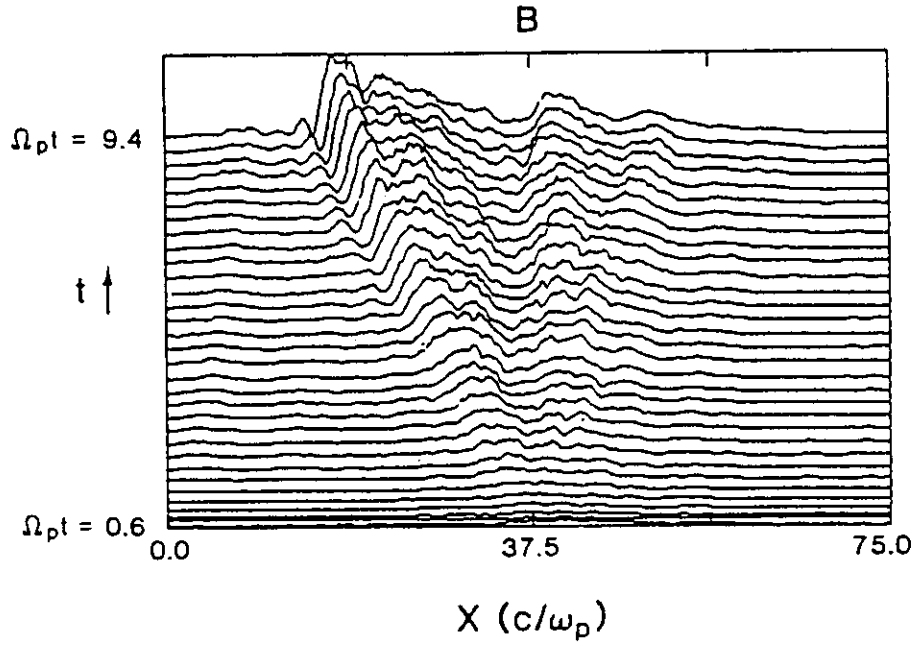

Figure 21: Wave splitting observed from computer simulation results (Omidi and Winske, 1990). This is similar to the G-Z results shown in Fig. 19.

Table 1: Jump conditions across four different types of discontinuities.

	Mass flux	Change in magnetic field	
Type of discontinuity	ρV_n	$[\vec{H}]$	
Contact discontinuity	0	$[\vec{H}_t] = 0$	$H_n \neq 0$
Tangential discontinuity	0	$[\vec{H}_t] \neq 0$	$H_n = 0$
Rotational discontinuity	$\neq 0$	$[H_t] = 0$	$H_n \neq 0$
Shock	$\neq 0$	$[\vec{H}_t] \neq 0$ $[H_t] \neq 0$	$H_n \neq 0$

f... ...l ... ...mal component of the field H_n are listed in column

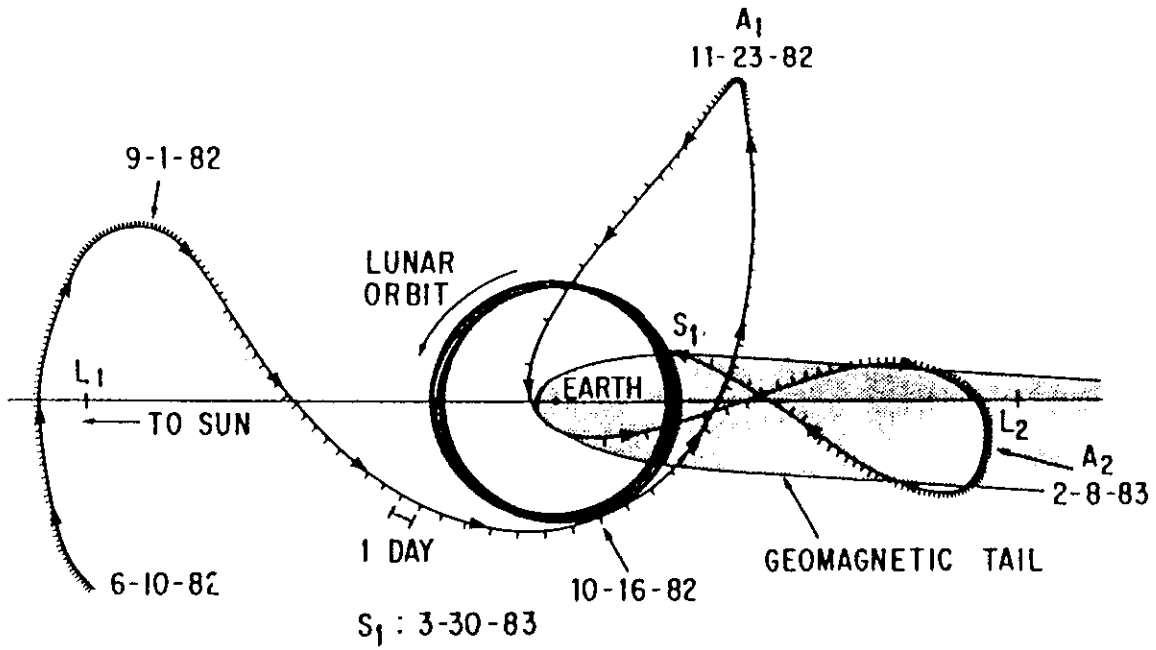
ISEE-3 GEOTAIL PASSES 1 AND 2
A1
11-23-82
9-1-82
LUNAR
ORBIT
S1
L1
EARTH
TO SUN
L2
A2
2-8-83
1 DAY
GEOMAGNETIC TAIL
6-10-82
10-16-82
S1 : 3-30-83

(a)

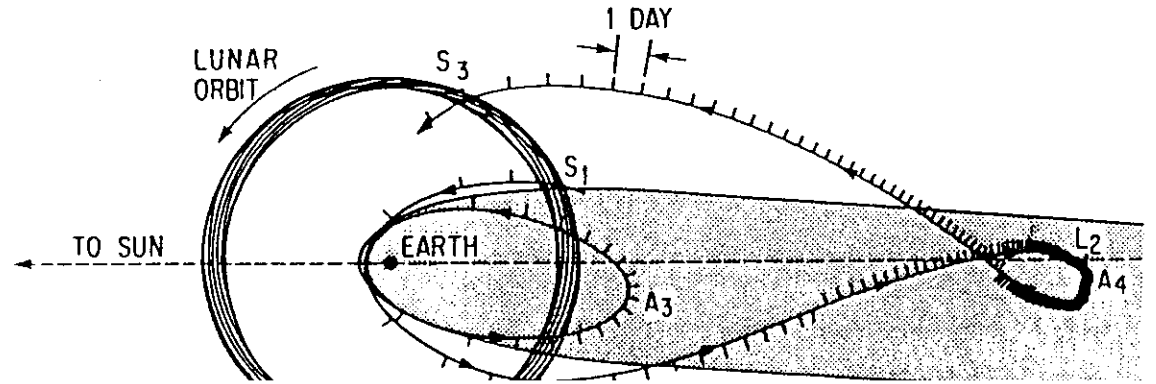
ISEE-3 GEOTAIL PASSES 3 AND 4
1 DAY
LUNAR
ORBIT
S3
S1
TO SUN
EARTH
L2
A4
A3

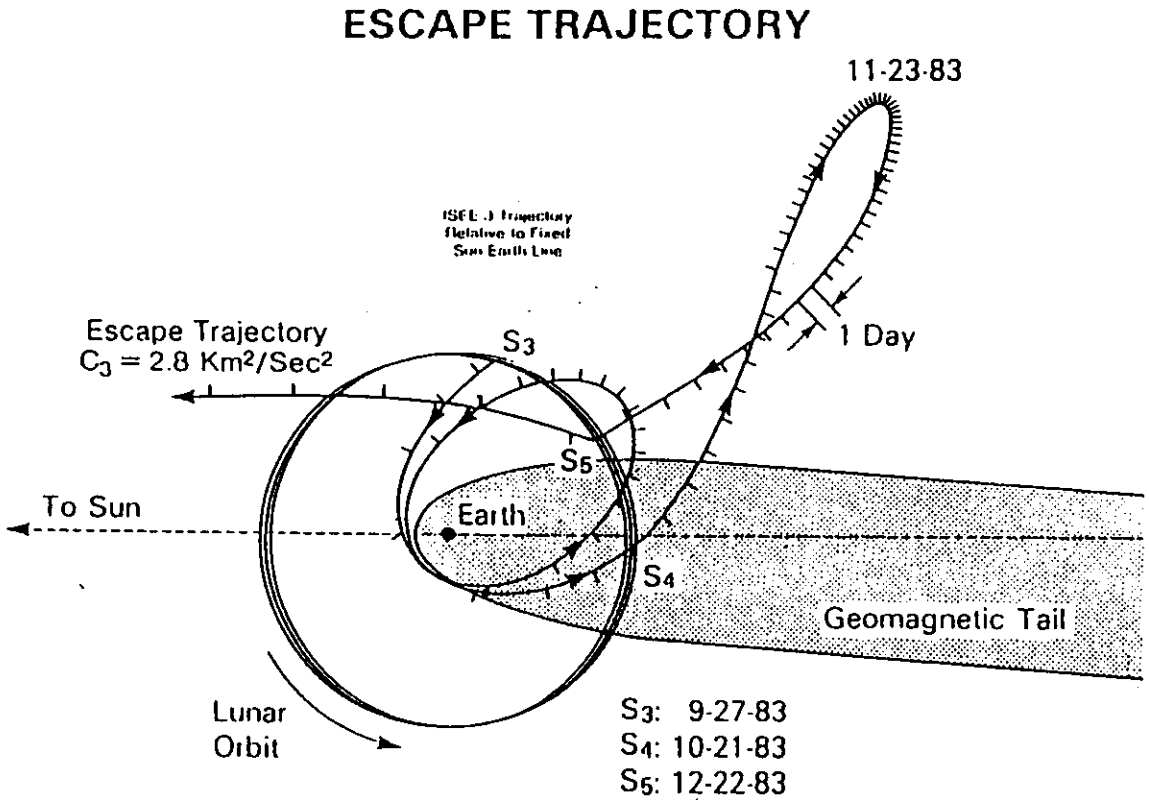

(c)

Figure 22: (continued).

ponent normal to its surface. There can be a significant change in the tangential field component crossing the discontinuity surface, however. A rotational discontinuity can be thought of as a sharply kinked Alfvén wave. A rotational discontinuity does have substantial mass flow across its surface, has a field component normal to its surface, and for isotropic plasmas, has a constant tangential field component magnitude.

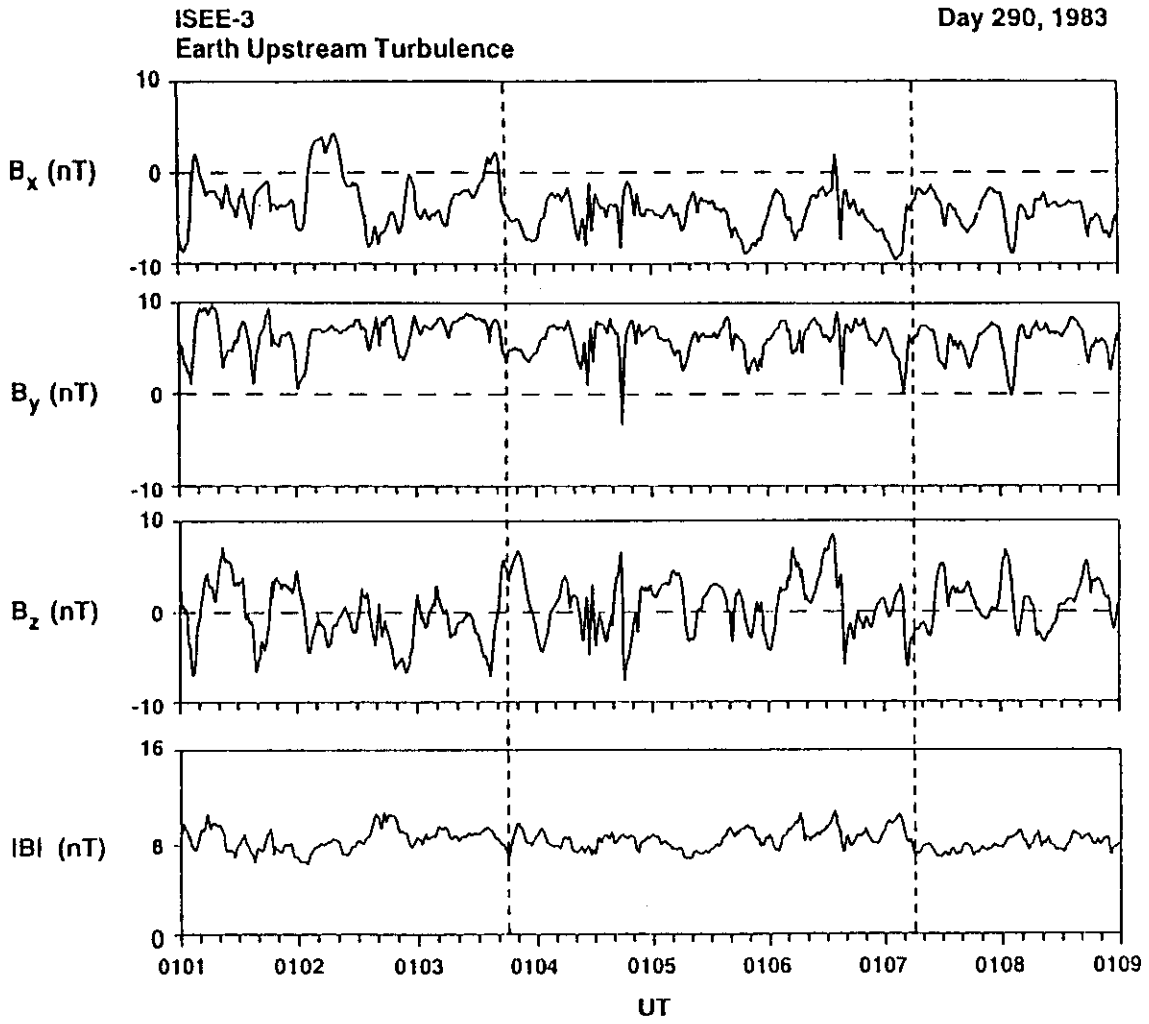

Figure 23: Turbulence-like magnetic fields detected within the Earth's downstream foreshock region.

of the measurements). As an example, out of thousands of discontinuities examined, a (tangential) discontinuity with no normal component (at levels

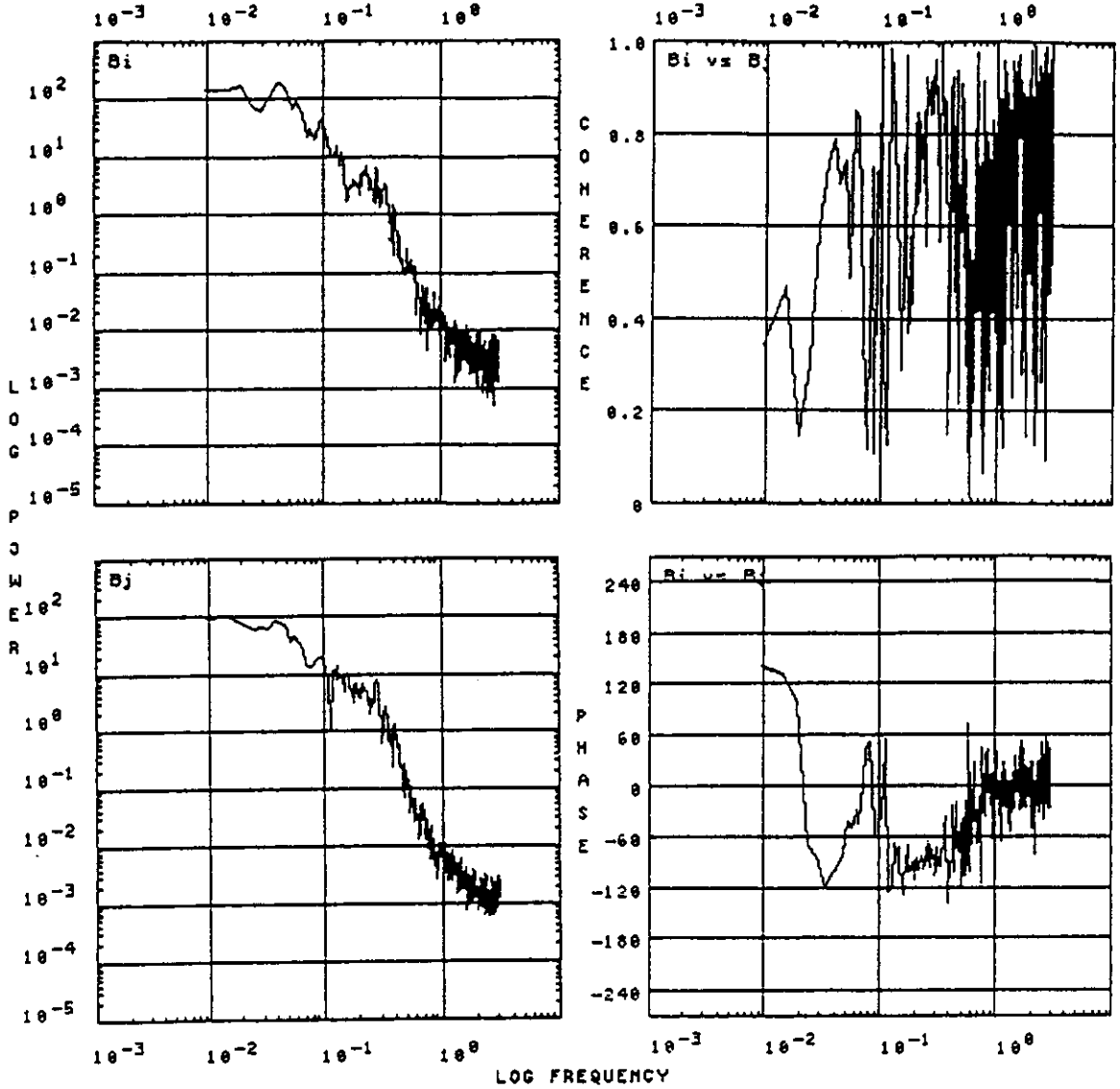

LOG POWER(nT^2/Hz) vs LOG FREQUENCY(Hz)

Frequency Bands: 633 Bands Averaged: 3
Bandwidth(Hz): 0.0048088 Resolution(sec): 0.164
Start: 83 290 OCT 17 01:03:44.881

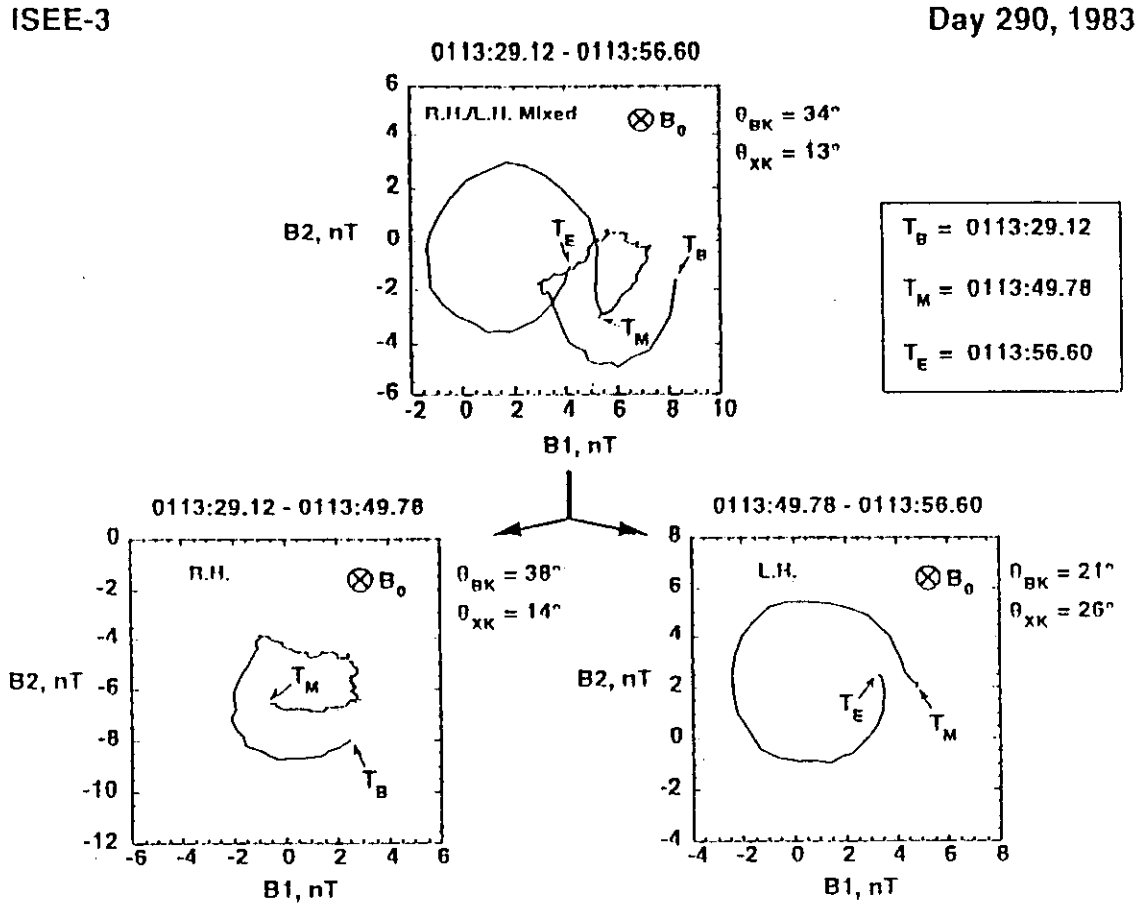

Figure 25: A right-hand circularly polarized wave immediately followed by a left-hand circularly polarized wave.

of discontinuity occurrence rates. The occurrence rates had fall-offs that varied exponentially with distance. It was concluded that this was due to a thickening of the discontinuity as a function of decreasing field strength. To normalize the rate to 1 AU, a factor $e^{(r-1)}/4$ was empirically derived, where r is in units of AU.

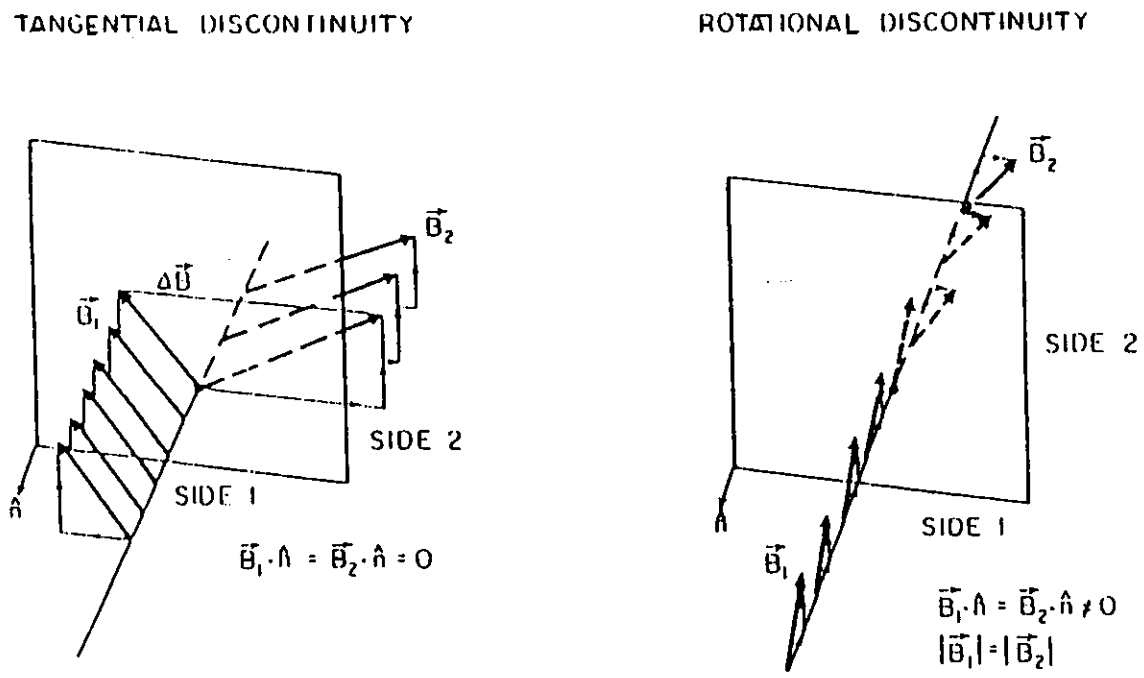

Figure 26: A schematic of an idealized tangential discontinuity (left-side) and a rotational discontinuity (right-side).

reaches a high enough latitude so that it is permanently immersed in the polar coronal hole stream, the rate of discontinuity occurrence determined by the TS method is ~150–200 day^{-1}, about 4 to 5 times that in the ecliptic plane at 1 AU. The primary cause of this relationship is shown in Fig. 30. This is an interval at large (negative) heliospheric latitudes where the solar wind speed is a constant ~700 km s^{-1}. The field components show a great deal of fluctuations due to the presence of Alfvén waves with $\Delta\vec{B}|/|B| \sim 1$ to 2. The waves are propagating outward from the sun (Tsurutani *et al.*, 1994). The high Alfvénic fluctuation levels (at 1 AU) in high speed streams was first pointed out by Belcher and Davis (1971). Figure 31 shows the

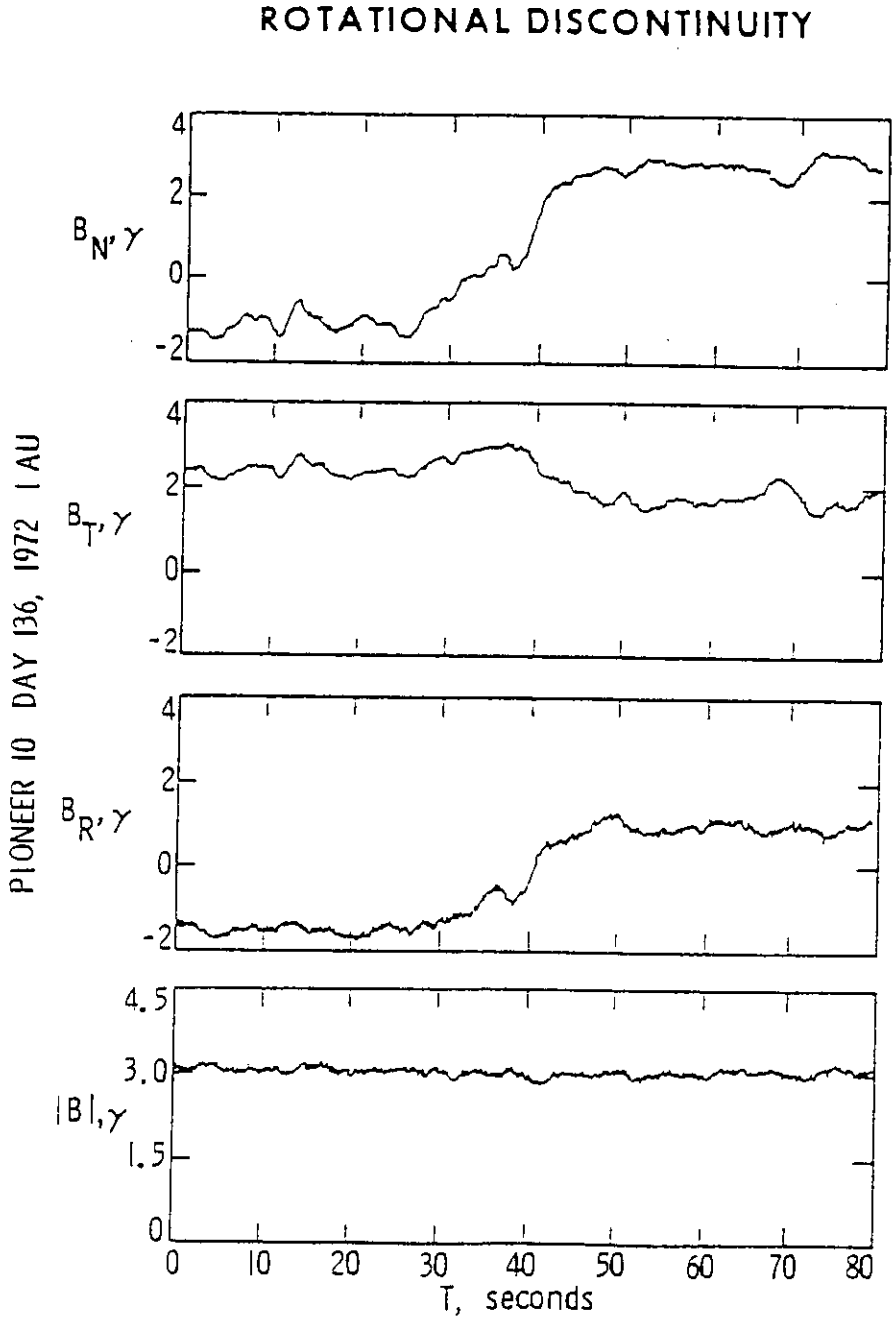
ROTATIONAL DISCONTINUITY
PIONEER 10 DAY 136, 1972 1 AU
B_N, γ
B_T, γ
B_R, γ
|B|, γ
4
2
0
-2
4.5
3.0
1.5
0
0 10 20 30 40 50 60 70 80
T, seconds

ROTATIONAL DISCONTINUITY

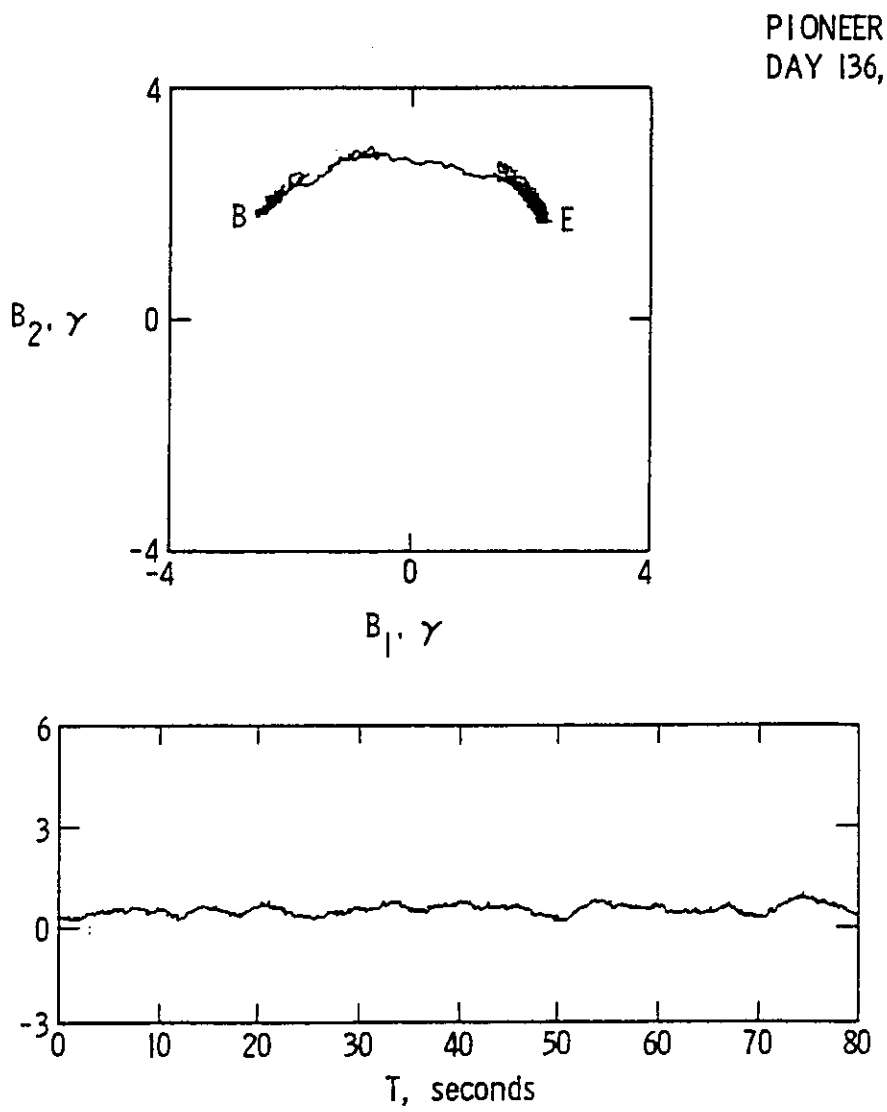

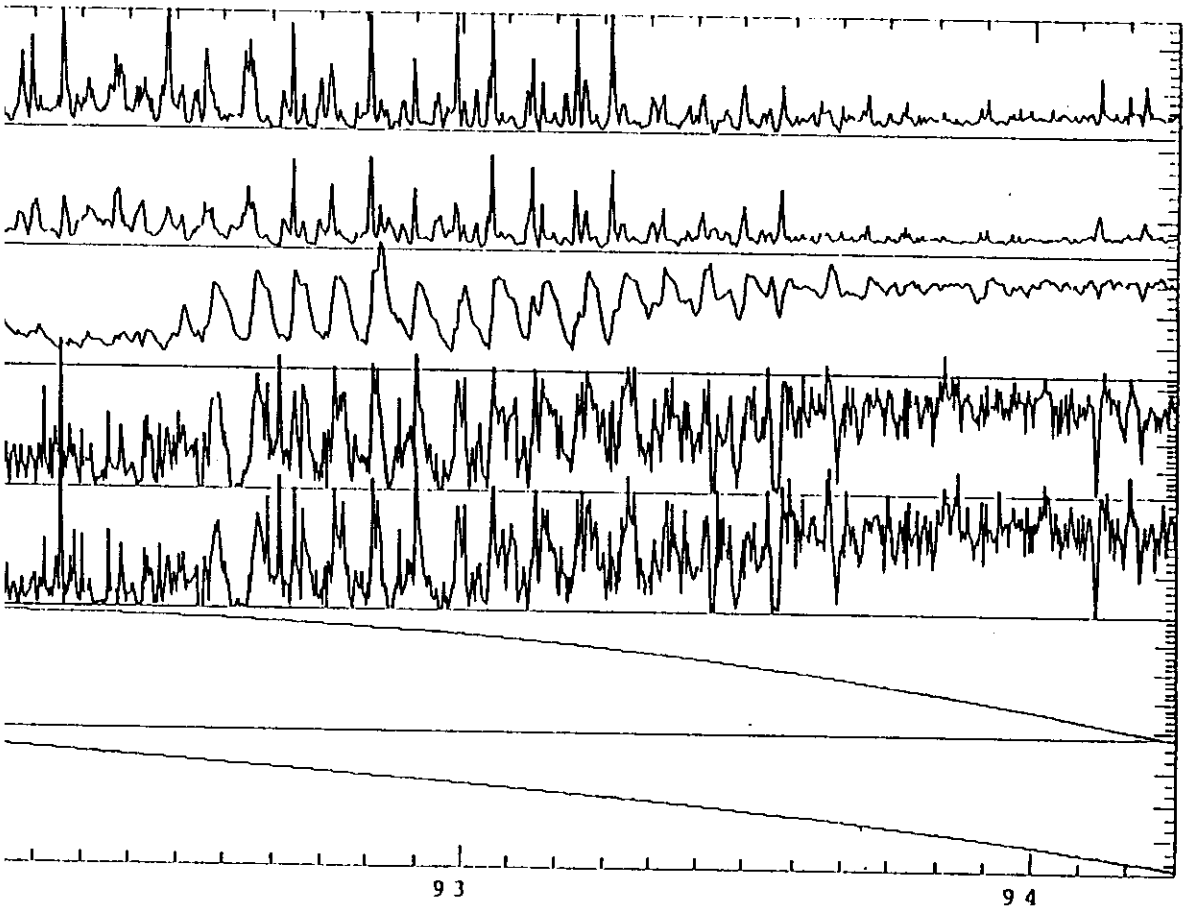

The rate of occurrence of discontinuities as a function of solar wind streams
graphic latitude).

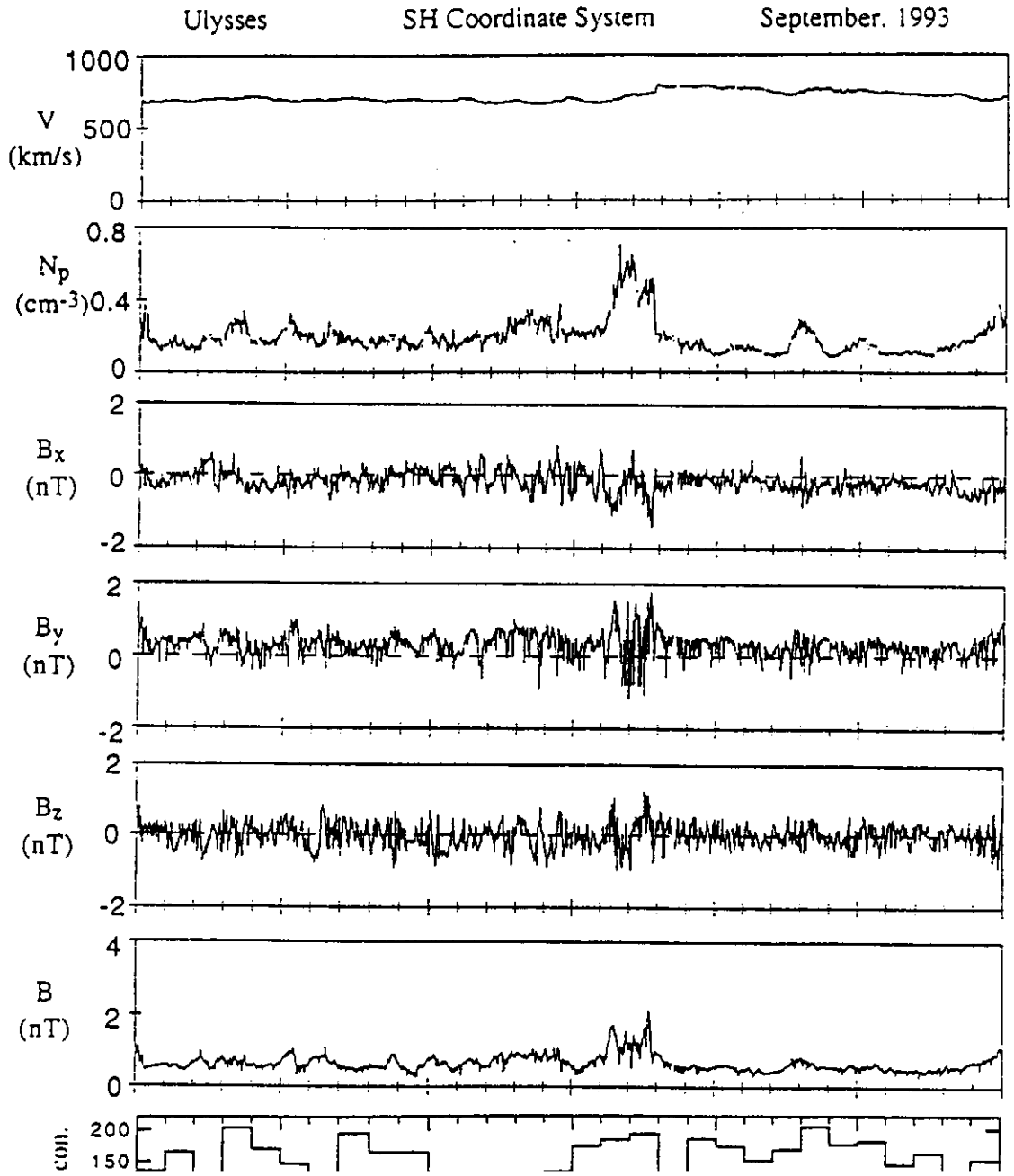
Ulysses
SH Coordinate System
September. 1993
1000
V
(km/s)
500
0
0.8
Np
(cm-3)0.4
0
2
Bx
(nT)
0
-2
2
By
(nT)
0
-2
2
Bz
(nT)
0
-2
4
B
(nT)
2
0
coll.
200
150

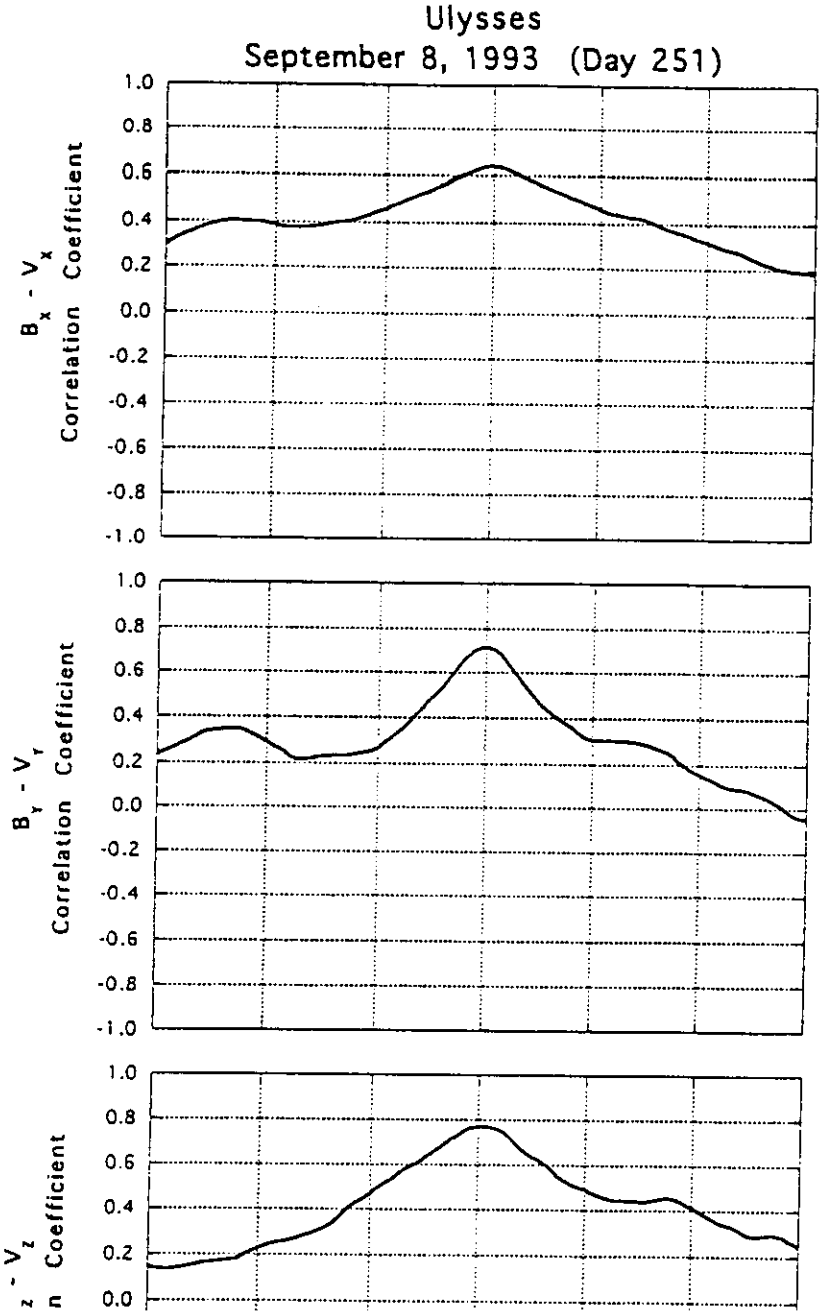
Ulysses
September 8, 1993 (Day 251)
$B_x - V_x$ Correlation Coefficient
$B_r - V_r$ Correlation Coefficient
$_z - V_z$ n Coefficient
1.0
0.8
0.6
0.4
0.2
0.0
-0.2
-0.4
-0.6
-0.8
-1.0

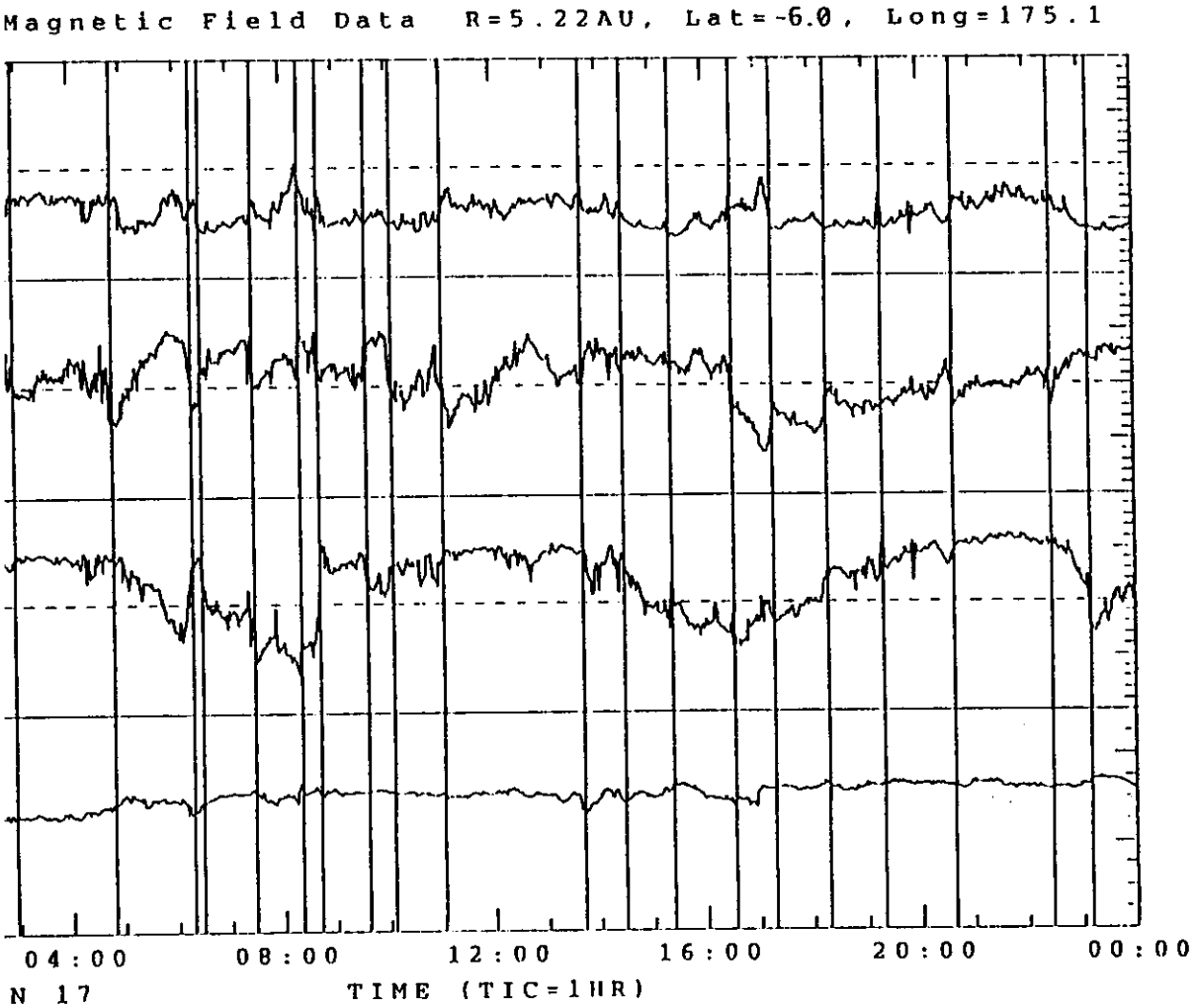

ure 32: Interplanetary discontinuities (vertical lines) and Alfvén waves.

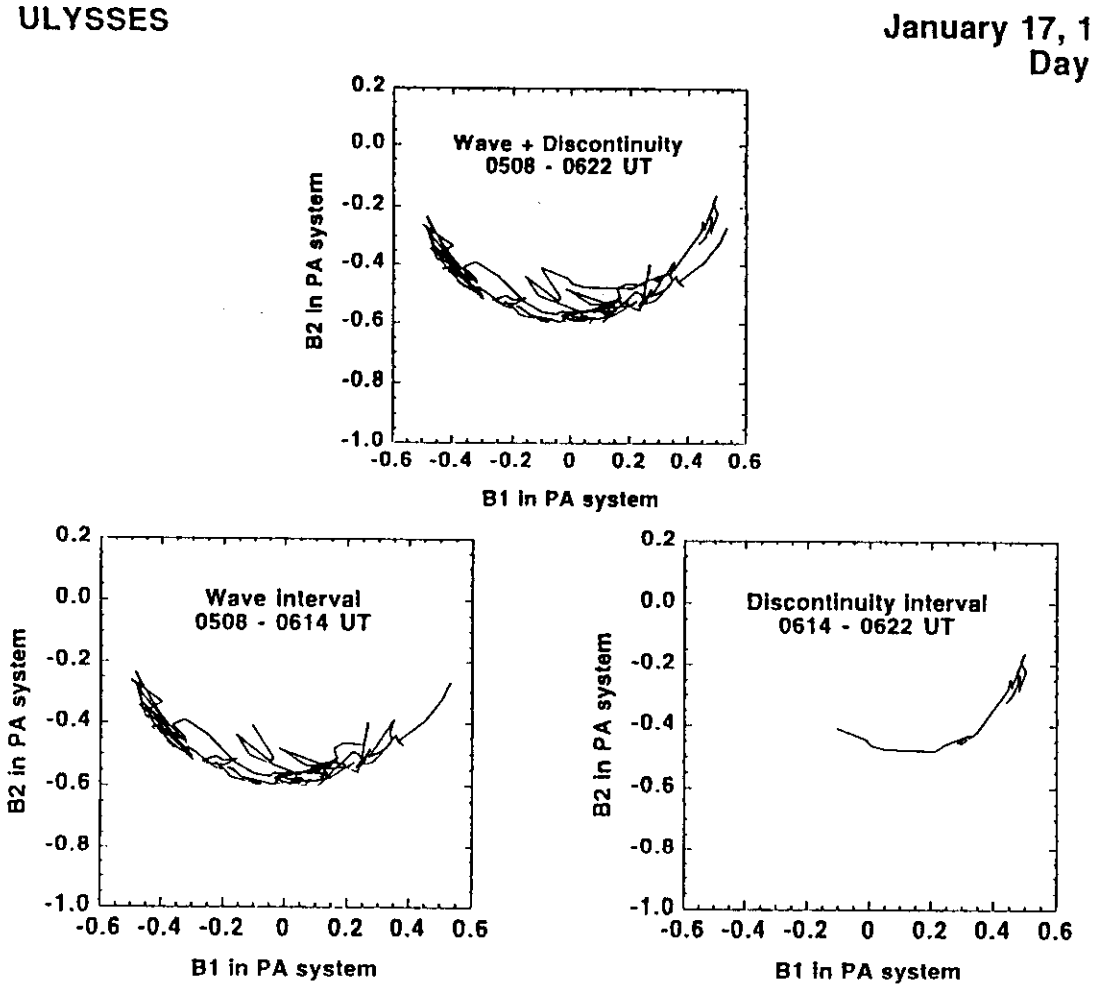

Figure 33: The phase relationship between the Alfvén wave and trailing discontinuity.

It appears as though the discontinuity is the phase steepened edge of an Alfvén wave, very much like the cometary and foreshock wave steepened fronts. However, at this time, it is uncertain whether the Alfvén waves

1.3 Conclusions

We have given selected examples illustrating the present status of LF nonlinear waves and turbulence. Nonlinear evolution of cometary, foreshock and interplanetary waves have demonstrated many fascinating examples, not all of which are theoretically well understood. Within these example, we do not find obvious cases of fully developed turbulence, however. This probably indicates that the plasma has not had enough time for wave-wave interactions to dominate the spectra. The only space plasma case where this seems possible is at comet Halley, where the scale sizes are the largest yet encountered (see Tsurutani *et al.*, 1995 for discussion) and perhaps in the downstream foreshock regions.

Acknowledgments. This work was supported by the Alexander von Humboldt foundation of Germany. We wish to thank J. Arballo and C. Ho at the Jet Propulsion Laboratory for help in parts of the data analyses and figure construction. Portions of this work were carried out at the Jet Propulsion Laboratory, California Institute of Technology, Pasadena, under contract with the National Aeronautics and Space Administration.

References

1) Belcher, J. and L. Davis, Jr., Large amplitude Alfvén waves in the interplanetary medium, 2, *J. Geophys. Res.*, 76, 3534, 1971.

2) Brinca, A. L., Cometary linear instabilities: From profusion to perspective, in Cometary Plasma Processes, ed. by A. Johnstone, *Am. Geophys. Un.* Press, Wash, D.C., 61, 211, 1991.

3) Chen, F. F., *Intro. Plasma Phys. Cont. Fus.*, Plenum Press, N.Y., 1, 1990.

4) Cohen, R. H. and R. M. Kulsrud, Nonlinear evolution of parallel propagating hydromagnetic waves, *Phys. Fluids*, B. 17, 2215, 1975.

5) Farquhar, R. W., D. Muhonon and L. C. Church, Trajectories and orbital maneuvers for the ISEE-3/ICE comet mission, *J. Astronaut. Sci.*, 1985.

11) Goldstein, M. L., H. K. Wong, A. F. Vinas, and C. H. Smith, Large amplitude MHD waves upstream of the Jovian bow shock: Reinterpretation, *J. Geophys. Res.*, 90, 302, 1985.

12) Goldstein, M. L., H. K. Wong, and A. Eviatar, Excitation of MHD waves upstream of Jupiter by energetic sulfur or oxygen ions, *J. Geophys. Res.*, 91, 7954, 1986.

13) Hoppe, M. M., C. T. Russell, L. A. Frank, T. E. Eastman and E. W. Greenstadt, Upstream hydromagnetic waves and their association with backstreaming ion populations: ISEE 1 and 2 observations, *J. Geophys. Res.*, 86, 4471, 1981.

14) Karamabadi, H., D. Krauss-Varban, N. Omidi, S. A. Fuselier and M. Neugebauer, Low Frequency instabilities and the resulting velocity distributions of pickup ions at comet Halley, *J. Geophys. Res.*, 99, 21541, 1994.

15) Kennel, C. F. and H. E. Petschek, Limit on stably trapped particle fluxes, *J. Geophys. Res.*, 71, 1, 1966.

16) Kojima, H., H. Matsumoto, Y. Omura and B. T. Tsurutani, A study of wave instabilities driven by cometary ions, *EOS*, 70, 1182, 1989.

17) Kojima, H., A study of wave instabilities driven by cometary ions, masters thesis, Kyoto University, 1990.

18) Landau, L. D. and E. M. Lifschitz, *Electrodynamics of Continuous Media*, V.8 of Course of Theoretical Physics, Addison-Wesley, 224, 1960.

19) Lepping, R. P. and K. W. Behannon, Magnetic field directional discontinuities: Characteristics between 0.46 and 1.0 AU, *J. Geophys. Res.*, 91, 8725, 1986.

20) Neubauer, F. M., K. H. Glassmeier, M. Pohl, J. Roederer, M. H. Acuna, L.F. Burlaga, N. F. Ness, G. Musmann, F. Mariani, M. K. Wallis, E. Ungstrup, and H. U. Schmidt, First results from the Giotto magnetometer at comet Halley, *Nature*, 321, 352, 1986.

21) Neubauer, F. M., K. H. Glassmeier, A. J. Coates, and A. D. Johnstone, Low-frequency electromagnetic plasma wave fields at comet P/Grigg-Skjellerup. Analysis and interpretation, *J. Geophys. Res.*, 98, 20937, 1993a.

22) Neubauer, F. M., et al., Preliminary results from the Giotto magnetometer experiment during the P/Grigg-Skjellerup encounter, *Astron. Astrophys.*, 268, L5, 1993b.

23) Omidi, N. and D. Winske, Steepening of kinetic magnetosonic waves into shocklets: Simulations and consequences for planetary shocks and comets, *J. Geophys. Res.*, 95, 2281, 1990.

24) Roberts, D. A. and M. L. Goldstein, *Res. Geophys. Supp.*, 932, 1991.

30) Smith E. J., and B. T. Tsurutani, Magnetosheath lion roars, *J. Geophys. Res.*, 81, 2261, 1976.

31) Smith, E. J., B. T. Tsurutani, D. L. Chenette, T. F. Conlon and J. A. Simpson, Jovian electron bursts: Correlation with the interplanetary field direction and hydromagnetic waves, *J. Geophys. Res.*, 81, 65, 1976.

32) Sonnerup, B.U. O. and L. J. Cahill, Jr., Magnetopause structure and altitude from Explorer 12 observations, *J. Geophys. Res.*, 72, 121, 1967.

33) Thorne, R. M. and B. T. Tsurutani, Resonant interactions between cometary ions and low-frequency electromagnetic waves, *Planet. Space Sci.*, 35, 1501, 1987.

34) Tsurutani, B. T., Comets: A laboratory for plasma waves and instabilities in Cometary Plasma Processes, Geophys. Monogra. Ser., 61, ed. by A. Johnstone, *Am. Geophys. Un.* Press, Wash. D. C., 189, 1991.

35) Tsurutani, B. T., B. E. Goldstein, M. E. Burton, D. E. Jones, A review of the ISEE-3 geotail magnetic field results, *Planet. Space Sci.*, 34, 931, 1986.

36) Tsurutani, B. T., C. M. Ho, E. J. Smith, M. Neubauer, B., E. Goldstein, J. S. Mok, J. K. Arballo, A Balogh, D. J. Southwood and W. C. Feldman, The relationship between interplanetary discontinuities and Alfvén waves: Ulysses observations, *Geophys. Res. Lett.*, 21, 2267, 1994.

37) Tsurutani B. T. and P. Rodriguez, Upstream waves and particles: An overview of ISEE results, *J. Geophys. Res.*, 86, 4319, 1981.

38) Tsurutani, B. T. and E. J. Smith, Hydromagnetic waves and instabilities associated with cometary ion pickup: ICE observations, *Geophys. Res. Lett.*, 13, 263, 1986.

39) Tsurutani, B. T., E. J. Smith, B. Buti, H. Matsumoto and A. Brinca, Discrete phase changes within nonlinear steepened magnetosonic waves: Comet Giacobini-Zinner, *Geophys. Res. Lett.*, 17, 1817, 1990.

40) Tsurutani, B. T. and E. J. Smith, Interplanetary discontinuities: Temporal variations and the radial gradient from 1 to 8.5 AU, *J. Geophys. Res.*, 84, 2773, 1979.

41) Tsurutani, B. T., R. M. Thorne, E. J. Smith, J. T. Gosling and H. Matsumoto, Steepened magnetosonic waves at comet Giacobini-Zinner, J. *Geophys. Res. Lett.*, 92, 11074, 1987.

42) Tsurutani, B. T., D. J. Southwood, E. J. Smith and A. Balogh, A survey of low-frequency waves at Jupiter: The Ulysses encounter, *J. Geophys. Res.*, 98, 21203, 1993.

43) Wu, C. S. and R. C. Davidson, Electromagnetic instabilities produced by neutral